UNIVERSITY OF NAPLES FEDERICO II

DOCTORATE IN

MOLECULAR MEDICINE AND MEDICAL BIOTECHNOLOGY

XXXV CYCLE

Immacolata Zollo

The role of biomarkers in Endometrial Cancer: first steps towards large-scale screening and personalized therapy

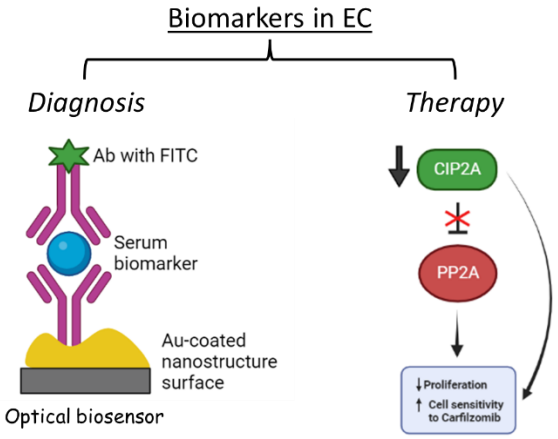

2019-2023

UNIVERSITY OF NAPLES FEDERICO II

DOCTORATE IN

MOLECULAR MEDICINE AND MEDICAL BIOTECHNOLOGY

XXXV CYCLE

The role of biomarkers in Endometrial Cancer: first steps towards large-scale screening and personalized therapy

Tutor

Prof. Giuseppe Castaldo

Co-Tutor

Dr. Maria Teresa Esposito

Candidate

Immacolata Zollo

2019-2023

INDEX

ABSTRACT

Endometrial cancer (EC) is the 6th most common cancer in women worldwide with an increasing mortality rate.
Currently, the diagnosis of this cancer is based on invasive and painful methods which are performed in presence of symptoms. If on the one hand the symptoms may indicate a more advanced stage of the tumor, on the other they may be linked to non-malignant pathological conditions. This particularly highlights the need for serum biomarkers that can both help the early detection of EC and avoid women without cancer to undergo an invasive test.
Many studies have shown significantly different levels of biomolecules between EC patients and healthy controls. However, the detection of these putative biomarkers is always based on traditional methods, like ELISA assays, that are not suitable for a point-of-care (POC) application.
An alternative detection method is represented by optical biosensors exploiting the phenomenon of *Metal Enhanced Fluorescence* (MEF). Biosensors are easy-to-use and cost-effective devices that allow multiplex real-time measurements of very low levels of biomarkers. They can be functionalized with antibodies or complementary nucleic acid probes depending on the target to be detected. The interaction between biomarkers and biorecognition molecules is converted into a quantifiable signal which is enhanced with the use of plasmonic nanostructured surface.
In the present study, optical biosensors have been developed and functionalized through *Photochemical Immobilization Technique* to detect serum diagnostic biomarkers of EC. The preliminary data obtained show the great potential of these devices in the use of a first level screening to distinguish a biological condition from a pathological one. Furthermore, fast-response analysis and multiplex measurements capability make optical biosensors powerful tools that would be well suited for large-scale screening.
Besides the role in the diagnosis, tumor markers can be used in the prognostic assessment and in the choice of therapeutic treatment when their levels affect the sensitivity to specific drugs.
In light of this, we additionally investigated the biological function of CIP2A, a protein found over-expressed in a variety of cancers, including EC, to assess its possible role as prognostic and therapeutic biomarker. We found that in leukemic cell models the down-regulation of CIP2A increases cell sensitivity to proteasome inhibitor Carfilzomib and affects cell proliferation. Although the effects we observed need to be confirmed in an endometrial cell model, these results suggest that CIP2A might be a promising target for cancer therapy.

1. BACKGROUND

1.1 Endometrial cancer: Epidemiology

Endometrial cancer (EC) is the 6th most common cancer in women worldwide. More than 417.000 cases of EC were diagnosed in 2020, mainly in North America and Western Europe. In particular, Poland had the highest rate of EC with an incidence of 26,2%, followed by Lithuania with 25,4%. (https://gco.iarc.fr/today/home).
The incidence of EC has shown an increase of 0,69% per year over the last three decades and is expected to rise further in the near future, as will the mortality rate (Zhang, 2021). In fact, if in 2020 it has been 97.370 the number of women who died from EC, according to the *International Agency for Research of Cancer* the mortality rate will increase by 62,1% in the next 20 years, thus reaching 157.813 deaths in 2040.
Significant disparities in incidence and mortality rates have also been highlighted between white and black women. Although the incidence of EC is lower among black women, they are more likely to die from the disease than white women (Jemal, 2021). Socioeconomic factors, like the unequal access to high-quality health care, may contribute to this discrepancy: EC is usually diagnosed at late stages in black women, when chances of a successful treatment are drastically reduced (Strömberg, 2019). However, several studies showed that the racial discrepancy persists even in an equal access healthcare system. This is in part due to the fact that black women have higher incidence of more aggressive histologic and molecular subtypes (Darcy, 2018; Goldberg, 2012). Yet, a worse outcome is still observed for them after stratifying by stage, grade and histology (Ali-Fehmi, 2015; Herzog, 2009; Zhu, 2021).

1.2 Anatomy of the uterus

Endometrial cancer originates from the cells of the inner layer of the uterus, the *endometrium* (Figure 1). The uterus is a highly vascularized hollow muscular organ located in the female pelvis between the bladder and rectum (Chaudhry SR and Chaudhry K, 2021; Peterson, 2022). It consists of two main parts:

- the *corpus* or *body* that is the upper part of the uterus. It starts directly below of the *Fallopian tubes*, 2 tubular ducts attached to the uterus on each side;
- the *cervix*, the lower end of the uterus that connects to the *corpus* via the *isthmus* and opens in the *vagina*.

The body of the uterus has three layers (Gasner and Aatsha, 2022):

- the *perimetrium*, also known as *serosa*, is the outermost, protective layer;
- the *myometrium* is the highly muscular middle layer. It is needed to push the baby out during the birth;
- the *endometrium* is the inner layer. It in turn consists of two layers:
    - the **basal layer** which contains the endometrial stem cells that generate the functional layer.
    - the **functional layer** which begins to grow at the beginning of each menstrual cycle and is shed with menstruation.

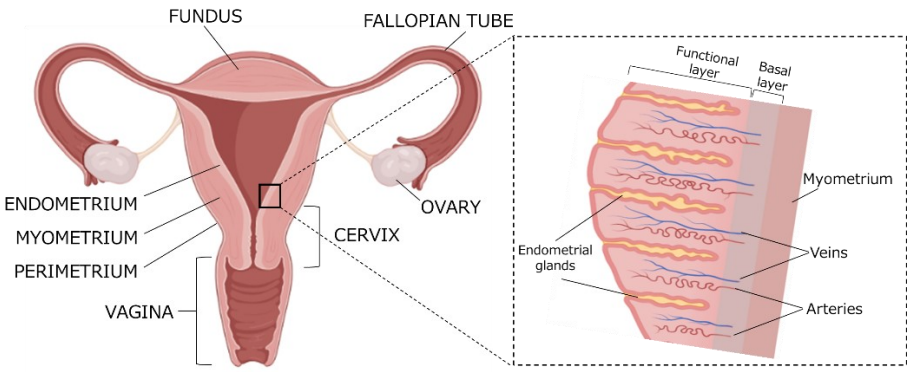

Figure 1. Anatomy of uterus. The uterus consists of two main parts, the *corpus* and the *cervix* which opens in the vagina. The *corpus* has three layers: the *endometrium* represents the inner one, from which the EC has origin. The zoom-in of *endometrium* on the right shows its two layers, the functional and the basal one. *Created in Biorender.*

1.3 Traditional classification of EC

Historically, endometrial cancer has been classified into two major groups, based on histological characteristics, hormone receptor expression, and grade (Table 1):

- **Type I**: is the most frequent, with a percentage of cases higher than 80%.
- **Type II**: accounts for less than 15% of cases of EC **(**Reventós, 2007).

The type I or endometroid EC is a low-grade subtype with a high or moderate differentiation, characterized by a hormone-receptor positivity and a favorable prognosis (Bokhman,1983).
It generally develops from an atypical endometrial hyperplasia (AEH) due to an increased or prolonged estrogenic exposure in younger women with obesity, hyperlipidemia and hyperestrogenism. In fact, obesity is recognized as one of

the strongest risk factors of type I EC since it triggers the "unopposed estrogen" mechanism. In this scenario there is an increased production of estrogen by adipocytes, associated to a decreased levels of progesterone that are not able to counterbalance the mitogenic effect of the former (Kurzer, 2002).
On the contrary, the type II EC is described as a non-endometrioid, high-grade and hormone-receptor negative tumor, characterized by an older age of onset and a poor prognosis. It typically develops from a previous endometrial atrophy and mainly shows a serous papillary or clear cell morphology (Bokhman 1983).
A significant association with lymphovascular invasion and nodal metastasis was also found in type II tumors and this fully explain its greater aggressiveness if compared to type I (Imran, 2020).

Table 1. Clinicopathologic characteristics of type I and type II EC.

	Type I	**Type II**
Incidence	>80%	<20%
Histotype	Endometrioid	Serous papillary; Clear cell
Estrogen-dependent	Yes	No
Age of onset	Pre-/Peri-menopausal	Post-menopausal
Precursor lesion	Atypical hyperplasia	Atrophy
Grade	Low	High
Prognosis	Good	Poor

Although this dualistic classification has been useful so far, it is oversimplified. High heterogeneity within each of the two types of EC that, at the same time, can share morphologic features has led the researchers to try to overcome the limitations of the traditional classification, coming to propose a molecular classification that turns out to have an improved diagnostic and prognostic accuracy.

1.4 Molecular classification of EC

In 2013, The Cancer Genome Atlas (TCGA) Research Network suggested a molecular classification based on a study of 373 cases of EC (Levine, 2013). According to genomic alterations, EC is categorized into four subtypes:

- **POLE ultramutated** that represents about 7% of EC. This subgroup is characterized by recurrent mutations in *POLE* gene, encoding the

exonuclease domain of polymerase-ε. Two main hotspots were recognized: Pro286Arg and Val411Leu.
POLE mutant tumors have shown a greater accumulation of spontaneous mutations especially in genes like *PTEN*, *PIK3R1*, *PIK3CA*, *FBXW7* and *KRAS* (Levine, 2013). The increased mutation rate is consistent with the role of this polymerase in the *nucleotide and base excision repair* mechanism during DNA replication. Despite the presence of high-grade malignancy and myometrium invasion, these tumors have a favorable outcome with a better progression free survival (Smit, 2016). This seems to be related to an enhanced intratumoral T-cell response (Church, 2015).

- **Microsatellite instability (MSI) - hypermutated**, found in approximately 25–30% of EC. It is characterized by defects in the *mismatch repair* (MMR) because of mutations or epigenetic silencing of genes involved in this mechanism like *MLH1*, *MSH2, MSH6*, *PMS2*. Recurrent frameshift deletions in *RPL22* and mutations in *KRAS* and *PTEN* have also been identified (Levine, 2013).

- **Copy number high (CNH) - serous like** that contains the more aggressive, high-grade tumors with the poorest prognosis. This group is characterized by extensive amplifications and deletions and recurrent mutations in *TP53*, *FBXW7* and *PPP2R1A* genes (Levine, 2013). Furthermore, frequent amplification of *CCNE1,* encoding the cyclin E1*,* and *ERBB2* are often found. Interestingly, FBXW7 is involved in the ubiquitin-mediated degradation of cyclin E1, the regulator of the transition from G1 to S phase. Therefore, mutations in *FBXW7* and amplification of *CCNE1* may both contribute to cyclin E1 overexpression, highlighting the role of this pathway in the development of CNH tumors (Shih, 2014).

- **Copy number low (CNL) - microsatellite stable**, also known as "no specific molecular profile" (NSMP) due to the absence of both mutation in *POLE* and *TP53* genes and deficient MMR mechanism. Although these tumors are generally represented by grade 1 and 2 endometrioid cancers with a low myometrial and lymphatic invasion, they are associated to a worse outcome (Broaddus, 2017). This is linked to the high mutation frequency in the exon 3 of *CTNNB1* gene, responsible for activating the WNT pathway (Zhang, 2014).

The assignment of an endometrial cancer to one of the four subtypes proposed by TCGA is based on complex and cost-prohibitive methods that require fresh-frozen samples, thus being unsuitable to the clinical practice. An alternative molecular classification system has therefore been developed. This approach,

known as *Proactive Molecular Risk Classifier for Endometrial Cancer* (ProMisE), uses the immunohistochemistry (IHC) to detect defective MMR proteins and mutant p53 and the sequencing to identify mutations in *POLE* gene (McAlpine, 2017).
The four molecular subgroups identified by ProMisE system are **DNA POLE**, mismatch repair-deficient (**MMR-d**), p53 abnormal (**p53abn**) and p53 wild type (**p53wt**), corresponding to POLE ultramutated, MSI, CNH and CNL genomic subtype respectively.
A low percentage of EC (3-6%) present more than one of the molecular characteristics listed above, thus being referred as "multiple classifiers". Most frequently, mutations in *TP53* can be found in the context of DNA POLE or MMR-d EC. These types of tumors maintain a good prognosis, suggesting that mutations in *TP53* are *passenger* events and do not affect the biological behavior of the cancer (Bosse, 2020).

1.5 EC Staging and treatment

Two are the systems used for staging endometrial cancer, the FIGO (*International Federation of Gynecology and Obstetrics*) system and the American Joint Committee on Cancer TNM staging system (Creasman, 2009). They both classify EC based on 3 factors: the size of the tumor, the spread to nearby lymph nodes and the presence of metastasis. The main characteristics of the four stages are reported below (Figure 2):

- **Stage I:** the cancer is confined to the *corpus* of the uterus. It could be found only in the endometrium or in less than one half of myometrium **(IA)** or there could be equal to or more than half myometrial invasion **(IB)**.

- **Stage II:** the tumor has spread to cervical stroma.

- **Stage III:** the tumor has spread beyond the uterus, with the involvement of the serosa **(IIIA)** and/or the vagina **(IIIB)**, pelvic lymph nodes **(IIIC1)** and para-aortic lymph nodes with or without metastasis to pelvic ones **(IIIC2)**.

- **Stage IV:** metastasis can be found in the mucosa of the rectum and/or bladder **(IVA)** or may have reached distant organs such as intestines, bones and lungs **(IVB)**.

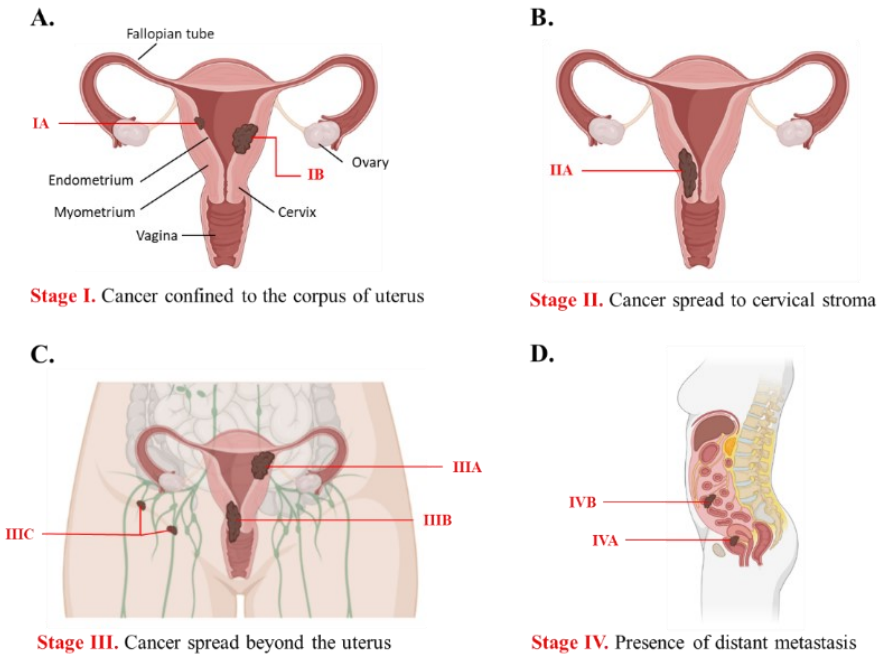

Figure 2. EC Staging. According to FIGO criteria four stages are distinguished in endometrial cancer: in stage I cancer is confined to the corpus of uterus **(A)**; in stage II it has spread to cervical stroma **(B)**; in stage III, it may involve the serosa, the vagina, pelvic and para-aortic lymph nodes **(C)**; in stage IV it has invaded rectum and/or bladder and distant metastasis can also be found **(D)**. *Adapted from Makker et al. Endometrial cancer. Nat Rev Dis Primers. 2021;7(1):88.*

The therapeutic approach is established mainly, but not only, according to cancer stage and grade. **Hysterectomy** is the first choice for women with a stage I. However, if the patient is still in her fertile age and wants to get pregnant in the future, progestin therapy can be considered to slow the cancer growth.

In case of a high-grade tumor, **pelvic radiotherapy** and/or **chemotherapy** are recommended after surgery to reduce the risk of recurrence (Creutzberg, 2021). When the cancer is in an advanced stage (III or IV), it has spread too far to be completely removed with surgery, thus **immunotherapy** and **targeted drugs** can be an option. The latter include *checkpoint inhibitors*, *DNA damage response inhibitors* and *cellular pathway inhibitors*. Although many inhibitors are currently under investigation to assess their effectiveness for the treatment of endometrial cancer, to date no drug has been approved to be used in the clinical practice (Gaillard, 2020).

1.6 EC Diagnosis

Abnormal vaginal bleeding is the most common symptom in women with EC, but it is far from being specific because it can be related to different causes (Wentzensen, 2018). Pelvic pain, abdominal distension and losing weight might be also present when the tumor is already in an advanced stage. When a woman has one of the above-mentioned symptoms, either **transvaginal ultrasonography** or **endometrial biopsy** are recommended as first tests for EC evaluation. The former is a cost-effective and less invasive test that is preferred as starting point in the diagnosis of EC. It allows to investigate the endometrial thickness and myometrial invasion. The most reliable *cut-off* value for endometrial thickness seems to be 5mm, with a sensitivity higher that 90% (Grady, 1998; Khan, 2002). However, a meta-analysis study by Mol and colleagues showed that reduction of the *cut-off* level to 3mm further increases the sensitivity, especially in postmenopausal women (Mol, 2010).

Despite the considerable advantages of transvaginal ultrasonography, this procedure may not be able to distinguish a benign condition from a malignant one and, therefore, an endometrial biopsy is then required (Davidson and Dubinsky, 2003). The endometrial tissue sample can be obtained by **Pipelle method** or **Dilation and curettage** (D&C) procedure. Pipelle method was proposed as an alternative of D&C because of its being less painful and requiring just a local, not a general, anesthesia, and equally maintaining a high sensitivity and specificity (Seyhan, 2021). Yet, if the sample obtained by Pipette method is not adequate or the results of biopsy are unclear, the D&C must be carried out. The two techniques have been also compared to evaluate their concordance to the final diagnosis made after the hysterectomy: D&C showed a higher accuracy in reflecting the final pathology (Kim, 2021). Another procedure used in the diagnostic assessment for EC is **hysteroscopy**, which may be combined to both Pipette biopsy and D&C. Biopsy under hysteroscopy, in fact, represents the gold standard for the diagnosis of EC, being able to improve sensitivity up to 99,2% (Khan, 2002) (Figure 3).

Additional tests to look for cancer spread are based on diagnostic imaging techniques. **Magnetic Resonance Imaging** (MRI) is widely used to evaluate myometrial and cervical invasion as well as lymph node metastasis (Iyer, 2009). Furthermore, when MRI is combined with **Positron emission tomography** (PET), it achieves a higher accuracy in the detection of cancer recurrence (Umutlu, 2018).

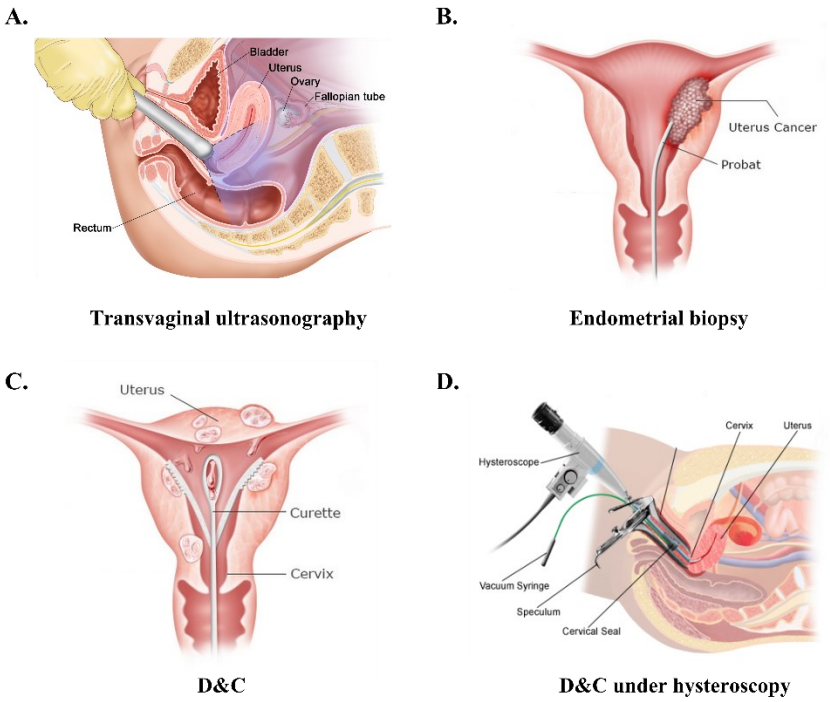

Figure 3. Tests for the diagnosis of EC. The main tests used for the diagnosis of EC are reported in the figure. The transvaginal ultrasonography requires an ultrasound transducer to be put into the vagina where it gives off sound waves and picks up the echoes as they bounce off the organs **(A)**. To obtain a tissue sample, either a small and flexible tube can be inserted through the cervix into the endometrium **(B)** or a curette may be passed after dilating the cervix **(C)**. Both procedures can be combined to hysteroscopy to improve the sensitivity of the test **(D)**.
Adapted from https://visualsonline.cancer.gov/details.cfm?imageid=9043 (A); https://www.cancerclinix.com/tests-to-detect-uterine-cancer/ (B and C); https://www.angelsfertility.com/services/diagnostic-hysteroscopy/ (D).

1.7 Limitation in diagnostic assessment of EC

The prognosis of EC is closely linked to early diagnosis. A study of 81.902 women with EC showed how much the 5-year survival rate is affected by the stage at diagnosis: it goes down from 89,6% in the case of diagnosis at stage IA to 21,2% in the case of diagnosis at stage IVB (Wright, 2010).
Consequently, the main limitation in the diagnostic assessment of EC remains the absence of a large-scale screening system for asymptomatic women like the Papanicolaou (Pap) test used for cervical cancer. Unfortunately, the Pap test is generally unable to detect EC, due to a very low sensitivity (Geldenhuys and Murray, 2007).

This particularly highlights the need for novel biomarkers that can help to clarify the cancer mechanism and to improve the EC diagnosis. Several attempts have been made to identify diagnostic or prognostic biomarkers that may be suitable for clinical practice, but none of them is currently routinely available.
Additionally, the identification of genetic mutations and aberrant signaling pathways might pave the way to the discovery of novel biomarkers for therapeutic purposes.

1.8 Biomarkers in EC

A biomarker is defined as "a biological molecule found in blood, other bodily fluids, or tissues that is a sign of a normal or abnormal process, or of a condition or disease" (www.cancer.gov/publications/dictionaries/cancer-terms/def/biomarker). A biomarker is considered as **diagnostic** if it allows to confirm or exclude the presence of a disease thanks to its significative difference between patients and healthy individuals. Instead, a **prognostic** biomarker reflects the disease outcome, so it can be favorable or unfavorable. Finally, **predictive** biomarkers can discriminate patients' response to a specific therapy, whereas **therapeutic** biomarkers are proteins that can be used as target for therapy.
Specifically, the ideal diagnostic or prognostic biomarker would be in blood, or other easily accessible body fluids, in order to avoid the use of invasive and painful diagnostic methods. Its expression should directly correlate to expression in the cancerous tissue and can be used with a diagnostic or prognostic purpose and may help in driving the choice of the therapeutic approach.
Currently, many research groups are studying the differences between protein and metabolite levels in the serum of women with EC. Guida and colleagues, for instance, identified a serum metabolomic signature of EC which allows not only the individuation of patients with EC, but also their discrimination by histotype (Guida, 2018).
Cancer antigen 125 (CA125) and Human epididymis protein 4 (HE4), instead, are the most widely studied protein as potential biomarkers for their known role in other gynecological tumors, especially ovarian cancer (Ducarme, 2019). Whilst CA125 has a low specificity for EC detection due to different benign conditions that may affect its levels like inflammation, endometriosis and pregnancy (Aggarwal and Kehoe, 2010), HE4 seems to be a more promising diagnostic and prognostic biomarker, both alone and in combination with other biomarkers (Crosbie, 2021).
HE4, YKL-40, DJ-1, EpCAM and miRNAs will be discussed in more detail in the following subsections as promising serum biomarkers for EC diagnosis.

In addition, PP2A and CIP2A, two proteins that have been found to play a role in the carcinogenesis of EC, will be presented as possible prognostic and therapeutic biomarkers for the treatment of this cancer.

1.8.1 HE4

Human epididymis protein 4 (HE4) is a small secretory glycoprotein firstly identified in the distal epididymis (Krull, 1991). It is encoded by the *WFDC2* gene on chromosome 20q12-13.1 and presents five distinct mRNA variants. Four of these (HE4-V0, -V1, -V2, -V4) are generated by alternative splicing mechanisms, whereas HE4-V3 utilizes an alternative promoter (Bingle, 2002).
HE4 is also known as WAP-four disulfide core domain 2 (WFDC2) for the presence of the WAP signature motif, consisting of eight cysteines that form four disulfide bonds at the core of the protein. Although most of the members of WFDC family act as protease inhibitors, the function of HE4 is still unclear. The gene is highly expressed in the upper airways, male and female reproductive tract and it was found overexpressed in different cancers, including EC (in more than 90% of cases) (Frierson, 2006). Interestingly, the chromosomic region mapping the gene for HE4 is known to be amplified in several cancer. This finding, on the one hand provides the potential mechanism responsible for the increase of HE4 expression, on the other hand suggests the role of this protein in carcinogenesis and tumor progression (Tremblay, 2006). Recent studies, for instance, showed its involvement in EC proliferation and invasion (Jiang, 2013). So far, HE4 is the most widely studied and promising blood diagnostic biomarker for EC, reaching a sensitivity of 81% and a specificity of 91% when the *cut-off* is 45pM (Ma, 2020). Furthermore, increased HE4 serum levels seem to be associated to advanced disease stage and deep myometrial invasion, making this protein also as a marker of poor prognosis (Li, 2013).

1.8.2 YKL-40

YKL-40, also named as chitinase-3 like-protein-1 (CHI3L1), was initially identified as a protein secreted by MG-63 osteosarcoma cell line (Price, 1992). YKL-40 is encoded by the *CHI3L1* gene, localized on the long arm of chromosome 1 (1q31–1q32), and belongs to chitinase family. It can bind to chitin, but, unlike the other members of this family, is lacking enzymatic activity (Recklies, 1993).

YKL-40 is known to be secreted by a variety of cells, including cancer cells. High serum levels are associated with poor prognosis and low overall survival in patients with metastatic cancer (Price, 2006). In fact, this protein can promote cell proliferation, migration and survival, beyond tumor angiogenesis and extracellular tissue remodeling (You, 2020). Although the molecular mechanism needs to be further elucidated, it seems that YKL-40 stimulates the coupling of the Syndecan-1 (Syn-1), a major proteoglycan on the epithelial cell surface, with the integrin $\alpha_v\beta_3$. This association activates FAK pY^{861} that mediates the angiogenic response by triggering the MAPK/ERK and PI3K/AKT pathways (Yan, 2009). Similarly, YKL-40 can induce the association of Syn-1 with integrin $\alpha_v\beta_5$ to activate FAK pY^{397} that results in the up-regulation of VEGF (Shao, 2011) (Figure 4). Moreover, it has been shown that YKL-40 inhibits E-cadherin, while enhances the activity of the metalloproteinase 9 (MMP-9). Both the absence of E-cadherin and the activation of MMP-9 promote tumor-cell invasion and metastasis, by decreasing cell-cell adhesion and degrading the extra-cellular matrix (ECM), respectively (You, 2020).
YKL-40 serum levels have been also evaluated in EC, showing a significant increase in patients compared to controls (Saygılı, 2016). According to a meta-analysis by Cheng *at al.* YKL-40 has a good diagnostic accuracy with a sensitivity of 74%, a specificity 87% and an AUC of 0.80 (He, 2014).

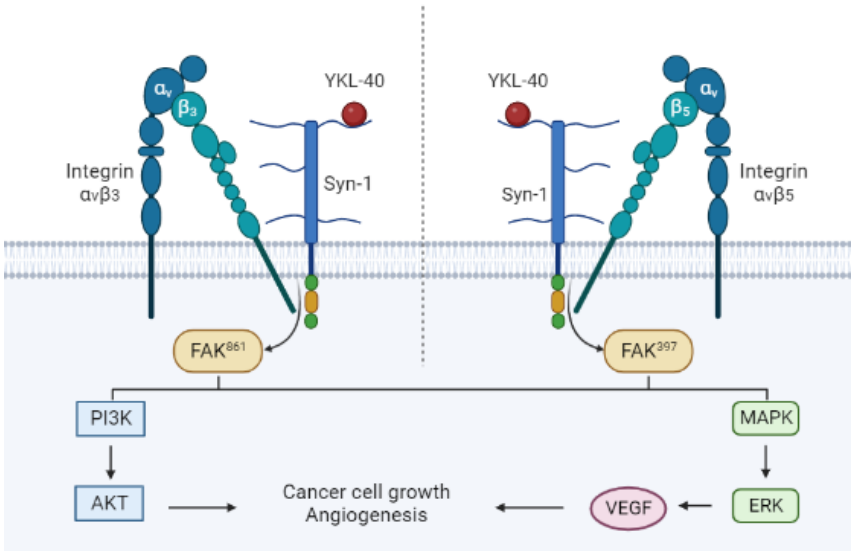

Figure 4. Effect of YKL-40 on cancer cell growth and angiogenesis. YKL-40 can promote cancer cell growth and angiogenesis by binding Syn-1 and thereby inducing its coupling with integrins. The association of Syn-1 with $\alpha_v\beta_3$ activates FAK^{861}, whereas that with $\alpha_v\beta_5$ activates FAK^{397}. FAK activates downstream signaling pathways like PI3K/AKT and MAPK/ERK which induces the upregulation of VEGF. *Adapted from Zhao et al. Chitinase-3 like-protein-1 function and its role in diseases. Signal Transduct Target Ther. 2020;5(1):201.*

1.8.3 DJ-1

DJ-1, also known as Parkinson's disease-associated protein 7 (PARK7), is a 189 amino acid protein isolated for the first time by Nagakubo *et al.* in 1997 (Ariga, 1997). The gene *PARK7* consists of 7 exons and is localized on the short arm of chromosome 1 (1p36.12–1p36.33). The protein exists as a dimer and is described as oncogene mainly for its role as negative regulator of PTEN (Mak, 2005), but there are a variety of oncogenic cellular mechanisms in which it is involved. For instance, DJ-1 may promote cell proliferation, survival and autophagy via activation of ERK1/2 and PI3K/AKT pathways (Oh and Mouradian, 2017), protect cells against hypoxia-induced cell death by blocking the VHL ubiquitination activity and thereby avoiding the degradation of HIF1α (Park, 2014), prevent apoptosis by repressing p53 transcriptional activity (Wang, 2008) (Figure 5).

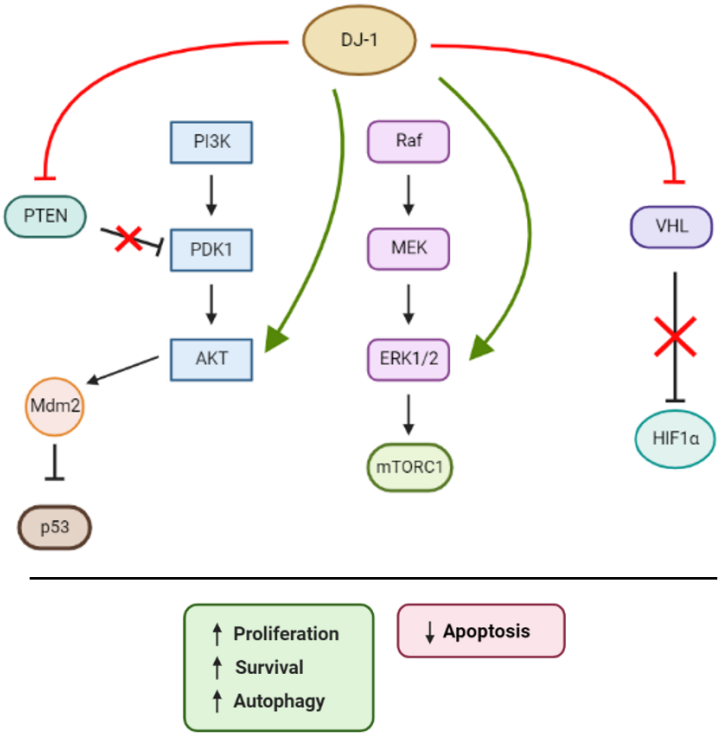

Figure 5. Major signaling pathways regulated by DJ-1. DJ-1 can promote proliferation, survival and autophagy while reduce apoptosis through the activation of PI3K/Akt and ERK1/2 pathways. In particular, DJ-1 increases Akt activity by both inhibiting PTEN and directly activating Akt. Akt can phosphorylate, among others, Mdm2 thereby increasing its nuclear stability which results in the proteasomal degradation of p53 and apoptosis decrease. In addition, DJ-1 activates ERK-mTOR pathway that results in increased autophagy and inhibits VHL, thus avoiding HIF1α degradation. *Created in Biorender.*

DJ-1 is frequently overexpressed in many cancer types. As regards EC, DJ-1 was at first found to be highly expressed in tumoral tissues compared to normal ones, also showing a correlation with cancer progression (Mei, 2013). Later, Morelli *et al.* suggested DJ-1 as a biomarker for the differential diagnosis between EC subtypes given that it is differentially expressed between the serum of patients with type I or type II EC (Costanzo, 2014). At the *cut-off* of 3654 pg/mL, DJ-1 detection has displayed a sensitivity and specificity of 89% and 90%, respectively (Lippi, 2018).

1.8.4 EpCAM

Epithelial cell adhesion molecule (EpCAM) is a transmembrane glycoprotein of 314 aminoacids that was identified for the first time in colon cancer in 1979. It consists of a large extracellular domain (EpEX) of 242aa, a single transmembrane domain of 23aa and a short intracellular domain (EpICD) of 26aa (Koprowski, 1979). The gene encoding for EpCAM is localized on chromosome 2 (2p21) and has 9 exons: exon 1 to 6 encodes for EpEX, exon 7 for transmembrane domain and exon 8-9 for EpICD (Litvinov, 1999). Besides its role as cell-cell adhesion molecule, many studies have revealed EpCAM function in cell signaling and proliferation. It is involved in the upregulation of c-Myc that in turn stimulates the transcription of genes like *cyclin A* and *E* to promote the cell cycle (Gires, 2004). In addition, EpCAM has a direct effect on *cyclin D* at the transcriptional level (Gires, 2013). Maetzel *et al.* further clarified the role of EpCAM in cell proliferation by revealing that it is a substrate for *regulated intramembrane proteolysis* (RIP). In fact, EpCAM undergoes to a double cleavage. The first is catalyzed by the metalloprotease ADAM17 and results in the release of EpEX that can act as a homophilic ligand for non-cleaved EpCAM to induce RIP. The second cleavage is carried out by Presenilin-2 (PS-2) and allows the release of EpICD that translocates in a complex with FHL2 and β-catenin to the nucleus, where induces transcription of target genes via TCF/Lef-1 *consensus sites* (Gires, 2009) (Figure 6). Considering that TCF/Lef-1 is the major regulator of c-Myc expression (Kinzler, 1998), this fully explains how EpCAM may upregulate this gene and thereby to induce cell proliferation. Moreover, since the regulation of EpCAM itself has been shown to depend on TCF4, EpICD may trigger a positive feedback loop on EpCAM expression (Wang, 2007).
High levels of EpCAM are frequently found in almost all cancers and they generally correlate with tumor progression (Mellstedt, 2012). In EC, on the contrary, EpCAM serum levels are usually higher in stage I-II compared to advanced ones. This finding makes EpCAM particularly interesting as diagnostic biomarker to detect EC in its very early stages (Torres, 2019).

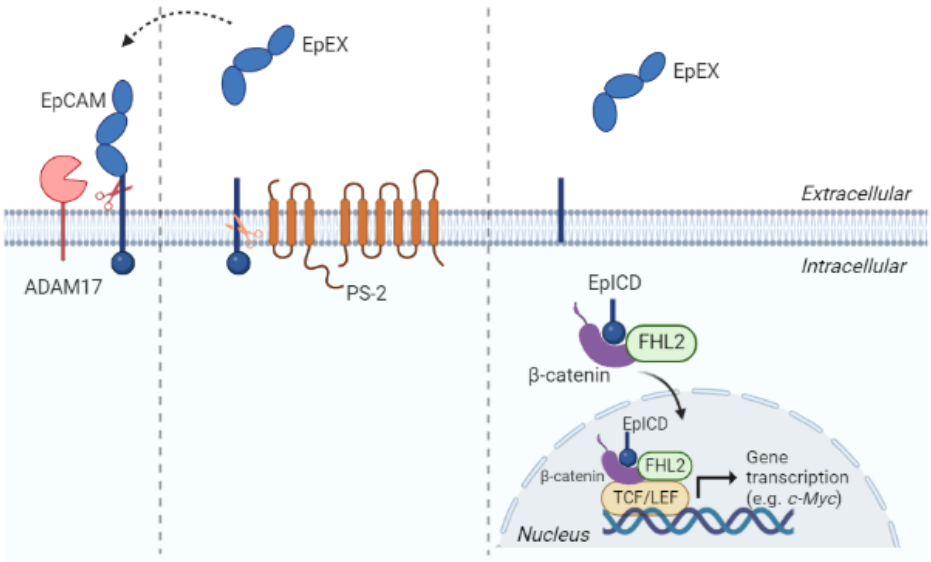

Figure 6. EpCAM signaling pathway. EpCAM is first cleaved by ADAM17 with the release of EpEX that can act as a homophilic ligand for non-cleaved EpCAM. Then, PS-2 carries out the second cleavage to release EpICD. EpICD, in a complex with FHL-2 and β-catenin, translocates to the nucleus where induces transcription of target genes (e.g., c-Myc) via TCF/Lef-1 *consensus sites*. *Adapted from Schnell et al. EpCAM: structure and function in health and disease. Biochim Biophys Acta. 2013 Aug;1828(8):1989-2001.*

1.8.5 miRNAs

MicroRNAs (miRNAs) are small non-coding RNAs of 18-22 nucleotides that play crucial roles in post-transcriptional regulation of gene expression. These molecules affect several biological processes by targeting mRNAs involved in cell proliferation, differentiation and apoptosis (Bartel, 2018). Over the past years, their role in cancer progression has been deeply studied. miRNAs are deregulated in most cancer types and their expression profile reflects tumor origin and stage (Lee and Dutta, 2009). In addition, circulating miRNAs can be found in almost all biological fluids, especially in plasma and serum, and they were shown to be highly stable and resistant to RNase degradation (Sohel, 2020). Thanks to their accessibility, stability and specific expression pattern, miRNAs have emerged as powerful non-invasive biomarkers for early cancer diagnosis and prognosis assessment.
Many studies investigated miRNA levels in serum of EC. Among others, miR-15b, miR-27a, miR-223 and miR-135b are particularly overexpressed in serum of EC patients compared to healthy individuals (Tu, 2014; Xiang, 2013; Masuzaki, 2014).

Although the regulation mechanism is still unknown, **miR-15b** is dysregulated in various malignant cancers. It is commonly considered a tumor suppressor since it promotes cell death by blocking the anti-apoptotic factor Bcl-2, inhibits cell proliferation by targeting cyclin E1 and D1, reduces angiogenesis by down-regulating the traditional VEGF receptor (VEGFR-2) (Zhang, 2016).

miR-27a has been shown to increase chemoresistance in different types of cancers (Sabatino, 2020; Chen, 2020; Xu, 2021). Recently, Hao *et al.* demonstrated that miR-27a can promote cell proliferation and migration of EC through the downregulation of the ubiquitin specific peptidase 46 (USP46) (Hao and Wang, 2021), a deubiquitinating enzyme with a tumor suppressive role (Gao, 2013).

miR-223 decreases the mRNA levels of FBXW7, thus increasing cyclin E levels and activity and resulting in genomic instability (Minella, 2010) that characterizes the subtype CNH of EC.

miR-135b seems to induce the development of EC by inhibiting FOXO1, a negative regulator of the PI3K/AKT signaling pathway (Liu, 2016).

Most research groups just compared miRNA levels between EC patients and healthy individuals, whereas some of them tried to find a correlation with cancer type to improve prognostic stratification of the patients (Perrone, 2022). For instance, the study by Ghazala *et al.* found higher levels of miR-27a in type I EC compared to type II (Abouzeid, 2021).

1.8.6 PP2A and CIP2A

Protein phosphatase type 2A (PP2A) is a Ser/Thr phosphatase consisting of 3 different subunits. The scaffold A subunit and the catalytic C subunit form the dimeric core of the holoenzyme. Both have two isoforms, α and β, of which the former is the most commonly expressed (Janssens and Goris, 2001). A third subunit, the regulatory B one, needs to be associated with AC core to determine the subcellular localization and substrate specificity. Indeed, there are 4 families of B subunits - $PP2A_B$ (B55/PR55); $PP2A_{B'}$ (B56/PR61); $PP2A_{B''}$ (B72/PR72); $PP2A_{B'''}$ (PR93/PR110) - and each of them counts several isoforms and splice variants. Different B subunits bind the core by interacting via the same or overlapping sites, thus being mutually exclusive (Janssens, 2013).
Among the targets of PP2A, there are proteins involved in cell proliferation, apoptosis and DNA damage response, all imbalanced processes in cancer. Considering that PP2A negatively controls cell proliferation as well as cell survival and is inactivated in many cancers, it has been proposed as putative tumor suppressor (Batra, 2013). Interestingly, the mechanism of PP2A

inactivation in EC differs between type I and II. Missense mutations in *PPP2R1A* gene, encoding the Aα subunit, have been identified mainly in type II EC, whereas they occur at a very low frequency in type I (Huntsman, 2011). The inactivation of PP2A in type I EC is primarily due to overexpression of the endogenous inhibitor CIP2A. In fact, the expression of PP2A endogenous inhibitors, together with transcriptional regulation of B and C subunits and post-translational modification of A, B and C subunits represent the key regulation mechanisms of PP2A activity (Kauko and Westermarck, 2018) (Figure 7).

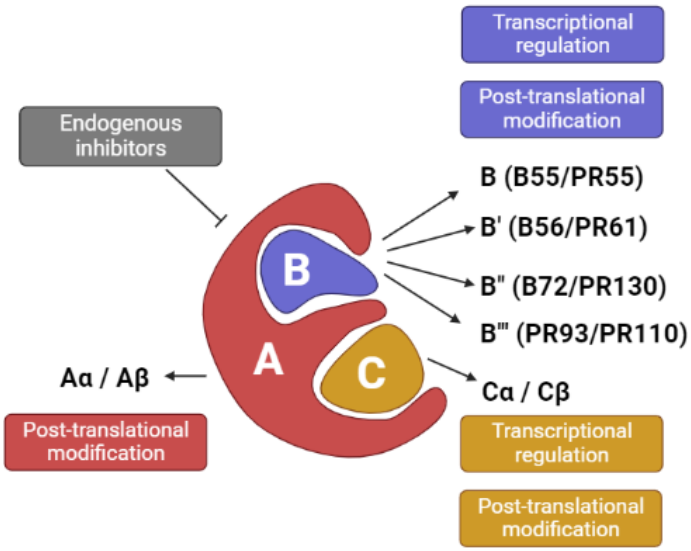

Figure 7. PP2A structure and regulation mechanisms. PP2A consists of three subunits: the scaffold A subunit (Aα/Aβ), the catalytic C subunit (Cα/Cβ) and the 4 classes of regulatory B subunits. The many regulatory B subunits determine the subcellular localization and substrate specificity of the phosphatase. Furthermore, PP2A activity can be regulated through expression of PP2A endogenous inhibitors, transcriptional regulation of B and C subunits and post-translational modification of A, B and C subunits. *Created in Biorender.*

Cancerous inhibitor of PP2A (CIP2A) is encoded by the gene *KIAA1524* and it was first described by Westermarck's group in 2007 (Westermarck, 2007). They identified CIP2A as a novel PP2A-interacting protein by coimmunoprecipitation analysis using an antibody against the A subunit of PP2A. Their study also showed that aminoacids between 461 and 533 of CIP2A are those required for the interaction since the binding to A subunit is impaired when they are deleted.

The mechanism by which CIP2A is able to inhibit PP2A is still unclear. However, it is known that CIP2A directly binds and stabilizes c-Myc , one of the main targets of PP2A, by preventing the dephosphorylation of its Ser62 and consequently its proteasomal degradation (Westermarck, 2007) (Figure 8).

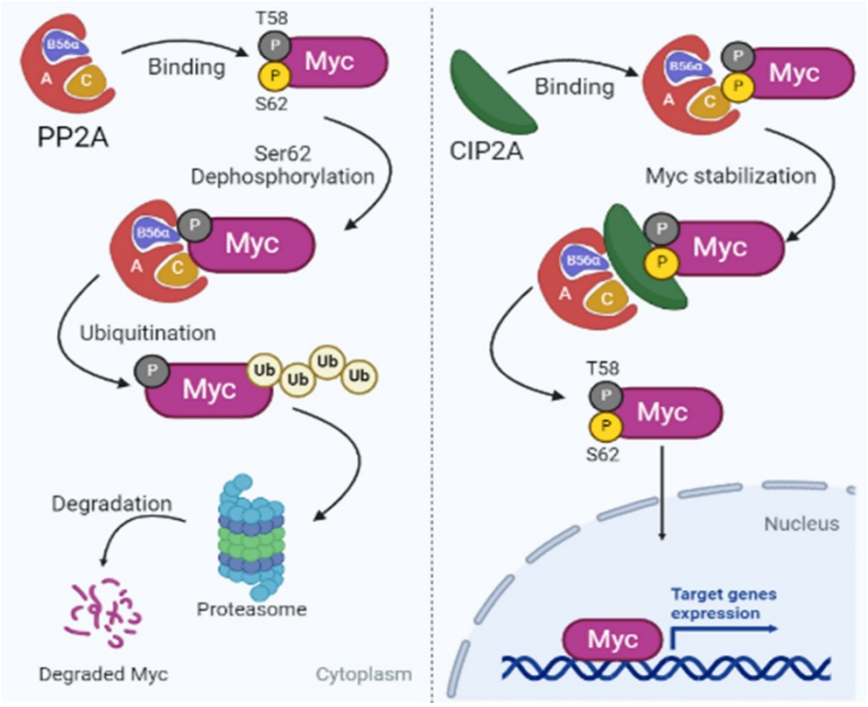

Figure 8. PP2A-CIP2A-c-Myc interaction. PP2A binds phosphorylated Myc via regulatory subunit B56α and dephosphorylates its Ser62. The dephosphorylation targets Myc for ubiquitination and proteasomal degradation (on the left). On the contrary, when CIP2A is present, it directly interacts with Myc and inhibits PP2A-mediated S62 dephosphorylation, thus allowing the stabilization of Myc. At this point, Myc is free to translocate into the nucleus and regulate the transcription of target genes (on the right). *Created in Biorender.*

CIP2A has been found over-expressed in a variety of cancers, including pancreatic, renal, ovarian, breast cancer and different forms of leukemia (Cao, 2013; Xu, 2011; Zhang, 2012; Westermarck, 2009; Clark, 2011).
Several studies have also shown that its overexpression is correlated to drug resistance, suggesting that CIP2A induces the upregulation of the P-glycoprotein drug efflux pump via the transcription factor E2F1 (Yang, 2011; Wang, 2016; Wang, 2019). Laine *et al.*, in fact, demonstrated that CIP2A increases the phosphorylation at Ser364 and therefore the stabilization of E2F1, which in turn induces the transcription of CIP2A, thus establishing a positive feedback loop (Westermarck, 2013).

Little can be found in literature on the relationship between CIP2A and EC. Two studies showed a significant increase of CIP2A expression in endometroid EC compared to normal endometrial tissues and this expression is strongly associated to FIGO stage and tumor grade (Akgün, 2020; Zhang, 2018). Furthermore, CIP2A down-regulation decreases cell proliferation and invasion, and increases apoptosis in endometrioid adenocarcinoma cell lines, suggesting that it could be a valid target for therapeutic compounds (Zhang, 2018).
For instance, erlotinib derivatives (tyrosine kinase inhibitors) as well as carfilzomib (proteasome inhibitor) are able to downregulate CIP2A by disrupting the interaction between its promotor and the transcription factor Elk1 (Chen, 2017a; Chen, 2017b), the main regulator of CIP2A expression in endometrial cancer cells (Rice, 2012).

1.9 Biomarker detection

Serum biomarkers have been proved to be good indicators of the onset and progression of a cancer. Their early detection can make the difference in the cancer outcome giving the possibility to start a therapy that has more chances to be successful. To reach this purpose, cheap, easy-to-use and fast-response methodologies are required for biomarker detection in the clinical routine.
Up to now, the detection of biomarker levels has been based on traditional methods, such as enzyme-linked immunosorbent assay (ELISA), electro-chemiluminescence immunoassay (ECLIA) and polymerase chain reaction (PCR). Although these assays are well tested and used in clinical practice, they present many limitations that hinder their use for a point-of-care (POC) application. Despite the good sensitivity and specificity, both ELISA and ECLIA assays are laborious procedures that require technical expertise and relatively high time and cost to be performed (Morimoto, 2018).
Therefore, the cancer diagnosis research is increasingly focusing on the development of analytical techniques that allow multiplex real-time measurements of very low levels of biomarkers. In fact, the parallel detection of different biomarkers is essential to improve the accuracy of a diagnosis (Patel, 2010).
In light of this, optical biosensors, which exploit the phenomenon of *Metal Enhanced Fluorescence* (MEF), could represent a highly sensitive and economical easy-to-use alternative for simultaneous detection of multiple analytes. The detection of very low quantities of analytes (by immobilization of antibodies on biosensors) using a few drops of blood as a starting sample, might be a better choice for early identification of the very first alterations that occur in the initial stages of EC and to draw a biomarker profile in the various phases of the disease.

1.10 Optical biosensors

During the last years, there has been a growing interest in the biosensors, transportable analytical devices consisting of biological mediators, coupled to suitable signal transducers capable of selectively and reversibly recording the concentration or the activity of different analytes in the sample. The device requires the efficient immobilization of antibodies, peptides, aptamers, or nucleic acids on the surface of a transducer responsible for the analyte recognition. Among biosensors, the development of biosensors that can be used for the detection of tumor biomarkers, thanks to their high sensitivity and multiplexing analysis ability, has greatly increased. Cancer biosensors can be functionalized with antibodies or complementary nucleic acid probes depending on the target to be detected. The interaction between biomarkers and biorecognition molecules is converted into a quantifiable signal. (Saxena, 2017) (Figure 9).

In particular, the use of plasmonic nanostructured surface in optical biosensors gives rise to the phenomenon of MEF: when a fluorophore is in close proximity of nanostructured metal surfaces, the emission of electromagnetic radiation from the analyte is enhanced (Cullum, 2015). Silver (Ag) and gold (Au) are the most widely used materials for MEF-based biosensor due to their characteristics, including electron conductivity and working range of wavelengths - from visible to near-infrared - (Li, 2019).

A critical parameter in this type of optical biosensors is the distance between the fluorophore and the metal nanoparticle: the fluorophore, in fact, should be far enough from the surface to avoid *quenching*, but at the same time it must be close enough to ensure that the MEF takes place. Thus, a distance of 5-90nm is required (Huang, 2012). This constraint is usually respected by introducing a spacer layer made of silica material, synthetic polymers or biomolecules. The use of biomolecules is highly advantageous for their biocompatibility and non-immunogenicity. Moreover, the functional groups of proteins such as the amino, thiolic and carboxylic ones, are particularly suitable as spacers because they also provide binding sites for metal nanoparticles or fluorophores (Möhwald, 2014).

Numerous applications of MEF-based biosensors are reported in the literature: biomarkers, toxins and pathogens have been detected with this system for early diagnosis, POC diagnosis and forensic applications (Saleem, 2020).

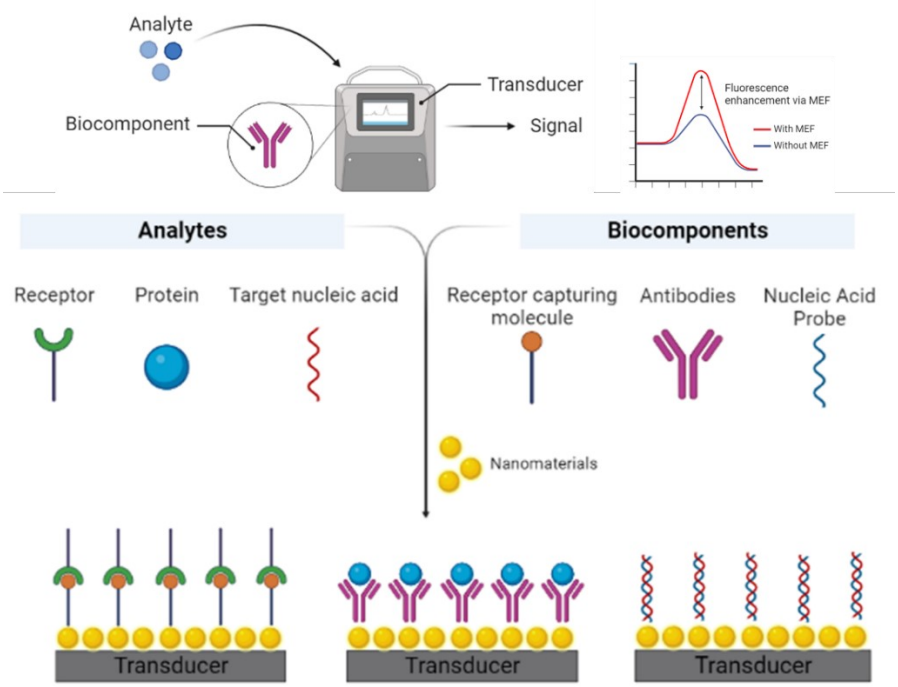

Figure 9. Optical biosensor designs based on MEF. For detecting receptors, nucleic acid or protein biomarkers, biosensors are functionalized with specific ligands, antibodies or complementary nucleic acid probes respectively. The use of nanomaterials, like gold nanoparticles, allows a significant enhancement of the fluorescent signal. *Created in Biorender.*

2. AIMS

There is currently no large-scale screening system for an asymptomatic population for the early diagnosis of endometrial carcinoma. Considering that prognosis and therapeutic approach are strongly linked to early diagnosis, it is crucial to have devices in which ease of use and rapid response must be combined with high analytical sensitivity and specificity.
Optical biosensors represent a valid solution to this request. They combine a sensitive biological element with a transducer capable of converting the recognition of the target analyte into an easily detectable optical signal, thus allowing rapid and reliable analyses even in poorly equipped laboratories. Furthermore, preliminary studies have shown the possibility of analyzing blood without any kind of pre-treatment or purification.
In light of this, the first aim of the present study is:

1) The development of optical biosensors for the detection of serum biomarkers, whose levels are altered in the case of EC.

Additionally, considering the role that biomarkers can play in the cancer therapy, we chose

2) To investigate the role CIP2A plays in cancer to assess its possible use as prognostic and therapeutic biomarker.

3. MATERIALS AND METHODS

3.1 Biological samples

Whole blood samples from healthy subjects were collected in tubes without anti-coagulant and centrifuged at 3500rmp for 15 minutes. Serum samples were separated from blood cells and stored at -80°C until the analysis.

3.2 Pollitt's method for AuNPs synthesis

A solution of 0,5 mL HAuCl4·H2O (24 mM) and 50 mL of ultrapure water was warmed on a hot plate at 150°C under vigorous stirring. During the boiling, 6 mL of sodium citrate dihydrate (39 mM) was added into the solution to induce the formation of gold seeds. After 2 minutes, 4,2 mL of HAuCl4·H2O (24 mM) was further added to trigger the growth of the gold seeds. The solution color moved from transparent to black and then to bright red within few minutes. Finally, the solution was cooled down for 2 hours by holding vigorous stirring. The as-synthesized AuNPs were spherical and showed an extinction spectrum with a narrow peak at ~530 nm and OD~8. The peak at 530 nm is characteristics for spherical AuNPs with average diameter of 35 nm.

3.3 UV-lamp

The UV source (Trylight®, Promete S.r.l.) consisted of two U-shaped low-pressure mercury lamps (6 W at 254 nm) in which a standard 10 mm quartz cuvette could be easily housed. The wrapping geometry of the lamps and the proximity of the cuvette are such that the irradiation intensity used for the Ab activation was approximately 0.3 W/cm^2.

3.4 ELISA assays

Serum HE4 and YKL-40 levels were analyzed using human-specific Quantikine ELISA kits (R&D Systems, Bio-Techne, USA), in accordance with the manufacturer's instructions. The assays were performed using anti-human HE4 or anti-human YKL-40 precoated 96-well strip plates. All serum samples

and standard solutions for calibration curves were analyzed in duplicate using 50 µL of sample and mean concentrations were calculated. HE4 and YKL-40 were analyzed using 2-fold diluted and 50-fold diluted samples, respectively. The concentration values (pg/mL) of both molecules were obtained by interpolating the absorbance values on the respective calibration curve.

3.5 Cell lines

All cell lines used in this study had previously been engineered by Dr. Yolanda Calle (University of Roehampton) to stably express the green fluorescent protein (GFP).
K562 cells (chronic myeloid leukemia cell line carrying BCR:ABL oncofusion protein, the product of t9;22) were grown in Roswell Park Memorial Institute medium (RPMI-1640) (Sigma) supplemented with 10% of Fetal Bovine Serum (FBS) and 100U/mL penicillin and 100µg/mL streptomycin. Kasumi1 cells (acute myeloid leukemia cell line carrying AML1:ETO oncofusion protein, the product of t8;21) were grown in RPM1, 25mM HEPES-modified and supplemented with 20% of FBS and 100U/mL penicillin and 100µg/mL streptomycin. Both cell lines were maintained in culture at 37°C and 5% CO_2 in fully humidified incubators.

3.6 Lentiviral infection

K562 cell line was infected with shRNA lentiviral particles (SHCLNV, Sigma) to knock-down CIP2A. A shScramble (SHC002V, Sigma), designed to target no known gene sequence, was used as a transduction negative control. Both viruses are based on the plasmid vector pLKO.p1(Sigma) carrying a puromycin resistance cassette to allow transduction selection of the cells and the establishment of stable clones.
Lentiviral particles were mixed with polybrene (5 µg/mL) and fresh medium into a final volume of 100µl and added to $2x10^4$ cells. The virus and cell suspension were centrifuged together (spinoculation process) for 15 min at 800rcf at 32°C to enhance viral binding to the target cells (Malim, 2000).
The same protocol had previously been used by Dr. Maria Teresa Esposito to establish stable clones of Kasumi-shScramble and Kasumi-shCIP2A.

3.7 Colony-formation assay

After 48h from infection, cells were seeded into a 24-well plate and cultured in the MethoCult medium (STEMCELL Technologies, M3231), a semi-solid methylcellulose-based medium, supplemented with 100U/mL penicillin and 100mg/mL streptomycin. Procedure was performed according to the manufacturer's protocol. Every 7 days, $2x10^3$ cells were re-plated for three times in presence of puromycin. At the end of each re-plating, the colony morphology was analyzed using EVOS™ cell image system, whereas the lentiviral transduction and transformation assay protocol (LTTA) was employed for their quantification. Later, cells were passed in liquid culture, according to the conditions above described.

3.8 Proliferation curve assay

For proliferation curve assay, 1×10^4 cells per well were plated in 200µL into a 96-well plate. Cell proliferation was measured every 2-3 days for 14 days by GFP fluorescence using a Fluorescent Microplate Reader at 495nm. The data are reported as RFU (Fluorescence Units) versus days of incubation.

3.9 Immunofluorescence

In order to evaluate the DNA damage, Kasumi-shScramble and Kasumi-shCIP2A were first treated with Daunorubicin and then fixed and incubated with appropriate antibodies. In brief, $1,5x10^5$ cells per well were seeded into a 24-well plate. After 24h, cells were splitted 1:2 and Daunorubicin was added at a final concentration of 25nM. Cells treated with DMSO were used as control. At 24h cells were collected and cytospun at 500rcf for 5 min onto glass slides. Cells were first fixed with PFA 4%, then permeabilized and blocked with a solution containing BSA 1%, FBS 10%, TBS 1X – Triton X-100 0,5%. Slides were washed three times in PBS 1X and incubated with primary antibody against phospho - Histone H2A.X (Ser139) (Millipore / JBW301) o.n. After 3 washes in PBS 1X, slides were incubated with secondary antibody and DAPI for 1h. Images were collected using EVOS™ cell image system.

3.10 Oxidative stress assay

Distinct concentrations of Daunorubicin (Sigma) were added to $4x10^4$ K562 and Kasumi cells to induce oxidative stress. After 48h cells were incubated with 250nM CellRox Deep Reagent (Thermo Fisher) for 1h before analyzing the samples by flow cytometry (BD Accuri™ C6 Flow cytometer). An excitation of 635nm was used for the CellRox Deep Reagent (collected on FL4 on Accuri C6) and one of 495nm for GFP (collected on FL1 on Accuri C6). The data are reported as MFI (Median Fluorescence Intensity).

3.11 Carfilzomib treatment and FACS

Distinct concentrations of Carfilzomib (Selleckchem) were added to $4x10^4$ K562 and Kasumi cells. The effect of the treatment on cell death was analyzed after 72h of incubation by Fluorescence-activated cell sorting (FACS), using GFP as a fluorescence-based cellular viability reporter. The samples were processed for analysis of apoptosis using BD Accuri™ C6 Flow cytometer.

3.12 Western Blot

Cells were lysed by sonication in RIPA buffer (10mM Tris-HCl pH 8, 1mM EDTA, 0,5mM EGTA, 140mM NaCl, 1% Triton X-100, 0,1% Sodium Deoxycholate, 0,1% SDS) supplemented with protease inhibitors (10µg/mL of aprotinin, leupeptin, antipain, soybean inhibitor and 1mM phenylmethylsulphonyl fluoride PMSF) and phosphatase inhibitors (50mM sodium fluoride NaF, 1mM sodium orthovanadate Na3VO4).
Soluble protein extracts were separated by SDS-polyacrylamide gel electrophoresis and transferred to PVDF membranes 0,2µm pore size (Amersham™) by elettroblotting.
Membranes were blocked with 5% non-fat dry milk and incubated with primary antibodies (Table 2) o.n.
Membranes were later incubated with horseradish peroxidase (HRP)-conjugated secondary antibody (1:10000 in 5% non- fat dry milk) for 1 hour at RT.
Signals were finally detected with chemiluminescent detection system (ECL Prime, Pierce) by using Odyssey ® Fc Imaging System, LI-COR Biosciences.

Table 2. Primary antibody used for the study.

Primary antibody	**Dilution**	**Company/ Catalogue number**
CIP2A (for Kasumi)	1:1000 in 5% BSA	Cell signalling/ 14805
CIP2A (for K562)	1:500 in 5% non-fat dry milk	Santa Cruz / 80662
c-Myc	1:500 in 5% BSA	Cell signalling / 9402S
Phospho c-Myc Ser62	1:500 in 5% BSA	Cell signalling / 13748
GAPDH	1:1000 in 5% non-fat dry milk	Cell signalling / 2118

3.13 RNA extraction and qRT-PCR

Total RNA was extracted using Isolate II RNA Mini Kit (Bioline) according to the manufacturer's instructions. 2 µg of total RNA from each sample was used to obtain double-strand cDNA with SensiFAST™ cDNA Synthesis Kit (Bioline) setting up the following reaction: primer annealing at 25°C for 10 min, reverse transcription at 42°C for 15 min, inactivation at 85°C for 5 min and final hold at 4°C.
Quantitative Real-Time PCR (qRT-PCR) was performed with the The StepOnePlus™ Real Time System instrument (Applied Biosystem).
For each PCR reaction, 10µL 2x SensiFAST™ SYBR® No-ROX Kit (Bioline), 0,8µM of each primer (listed in Table Y) and 20ng of the cDNA were used.
The reaction was set up as follows: initial holding stage 95°C 2 min, 40 amplification cycles with three steps - 95°C 5 seconds (denaturation), 60°C 10 seconds (annealing), 72°C 20 seconds (extension) -, dissociation stage (95°C 30 seconds, 65°C 30 seconds, 95°C 30 seconds) and cooling holding at 40°C.
Relative gene expression was quantified by using the Pfaffl formula that takes into account the differences in primers efficiencies, previously evaluated, to increase reproducibility (Pfaffl, 2001).

Table 3. List of primers used for the study.

CIP2A Fw	5' - ACC CCA ACA TAA GTG CTT CAC - 3'
CIP2A Rev	5' - CTG TGA GGA GCT TCT TTT TG - 3'
GAPDH Fw	5' - AGG TGA AGG TCG GAG - 3'
GAPDH Rev	5' - GAG GTC AAT GAA GGG - 3'

3.14 Statistical analysis

Results are reported as mean ± standard deviation (SD). Data were analyzed by 2-way Anova test or t-test (qRT-PCR). Statistical analyses were carried out using GraphPad Prism software 8.0 and the difference was considered significant when $p < 0.05$.

4. RESULTS

4.1 Development of optical biosensors

The present study was carried out in collaboration with the Department of Physics "Ettore Pancini". We developed optical biosensors for the detection of serum biomarkers, whose levels are altered in the case of EC.

4.1.1 Nanostructure fabrication

The optical biosensors we developed are based on gold-coated nanostructure surfaces. Once the gold nanoparticles (AuNPs) were synthesized according to the Pollitt's method, they were randomly immobilized onto a glass substrate by adsorption via electrostatic interactions. The procedure we used includes the four steps schematically shown in Figure 10A. (a) The glass coverslips (Knittel Glass, Thickness No.1, 24 × 60 mm) were cleaned by sonication for 5 min in 2-propanol and ultrapure water sequentially. The top glass surface was activated by oxygen plasma treatment (1.4 mbar pressure, 150 W power, 4 min), thus leading to its oxidation and to the formation of silanol bonds (Si-OH-), which served as bonding sites for subsequent silane molecules. The silanols provided the top glass surface with hydroxyl functionalities and a consequent high negative charge. (b) The activated coverslips were incubated with a 0,5% (v:v) solution of (3-Aminopropyl)triethoxysilane (APTES) in water for 45 minutes at room temperature in order to form a thin layer of positively charged amino-terminated silanes on the glass surface. The substrates were extensively rinsed by ultrapure water after the APTES incubation to avoid the formation of silane multilayer which would trigger AuNPs aggregation in the subsequent step. (c) The silanized substrates were incubated for 3 hours with a AuNP solution (OD 8). The electrostatic interaction between the negatively charged citrate capping of AuNPs and the positively charged amino groups of silanes promoted the immobilization of the AuNPs onto the silanized substrate. The substrates were then extensively rinsed by ultrapure water and gently dried by a nitrogen spray gun. (d) A low-pressure oxygen plasma treatment (0.8 mbar pressure, 200 W power, 30 min) etched the free citrate ligands and silane layer leaving the bare AuNPs strongly anchored to the substrate.
Considering that the immobilization of AuNPs is random, and consequently their distribution is different for each glass substrate, is important to check the absorption spectrum of the nanostructure (Figure 10B). Figure 10B also shows a typical SEM image of the resulting nanostructure.

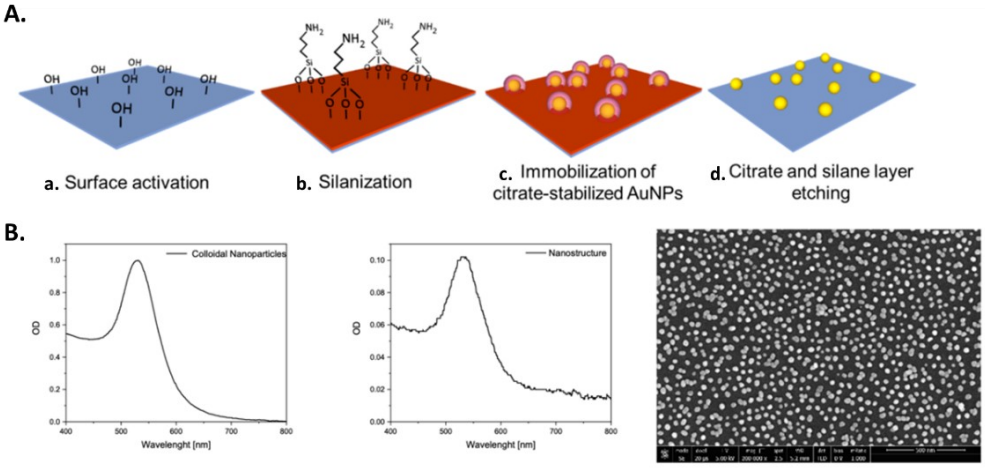

Figure 10. Nanostructure fabrication. A) Schematic representation of the procedure. The glass surface is firstly activated through oxidation (a). The OH-groups allows the bonds with the silane molecules to form a positively charged layer (b). The electrostatic interaction between the negatively charged citrate capping of AuNPs and the positively charged amino groups of silanes promoted the immobilization of the AuNPs onto the silanized substrate (c). Finally citrate and silane layer is etched through a low-pressure oxygen plasma treatment (d). **B) Absorption spectrum and SEM image of the resulting nanostructure.** Both colloidal nanoparticles (on the left) and the nanostructure (in the middle) show the absorption peak at 534nm.

4.1.2 Microfluidic system

The microfluidics consists of a supporting basement housing three "active" fluidic elements bringing canals, inlets/outlets, and a well of diameter 4 mm and volume 30µL. (Figure 11 a-b). Furthermore, we designed a custom microfluidic system geometrically equivalent to a standard 24-multiwell microplate in view of measurements to be performed by PHERAstar FSX instrument (Figure 11c).
The microfluidics as well as the mask were designed by Sketchup software and 3D-printed in PLA.

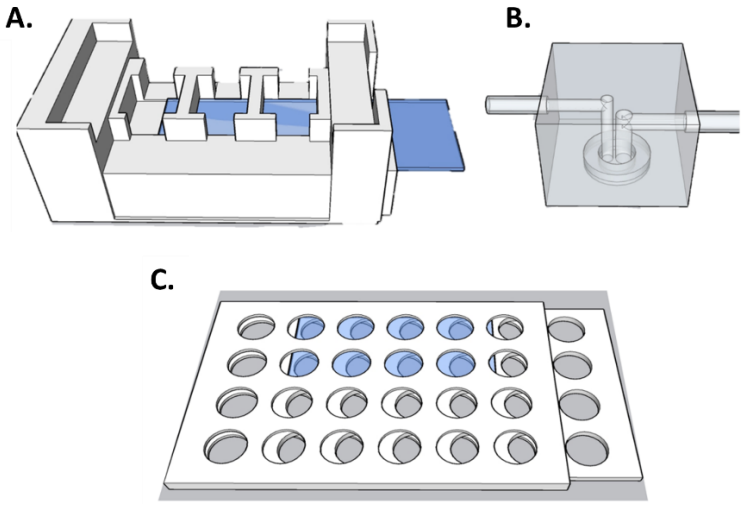

Figure 11. Microfluidic system design. The glass surface is lodged in a supporting basement housing three "active" fluidic elements **(a)** and a well of diameter 4 mm **(b)**. In **(c)** is represented the customized mask geometrically equivalent to a 24-multiwell microplate that was employed to perform the measurements by the PHERAstar FSX instrument.

A couple of cylindrical magnets (diameter 30 mm, height 10 mm) positioned into the bottom and top walls of the supporting basement guarantee the wells watertightness. A peristaltic pump and 0,8 mm silicone tubes for biological samples were employed, resulting in a total circulating volume of ~500µL. A preliminary kinetic study in which solutions of IgG (2 µg/mL) were flowed onto the nanostructure revealed that a flow rate of ~220 µL/min and a flow time duration of 15 min guaranteed the optimal fluidic efficiency (Figure 12).

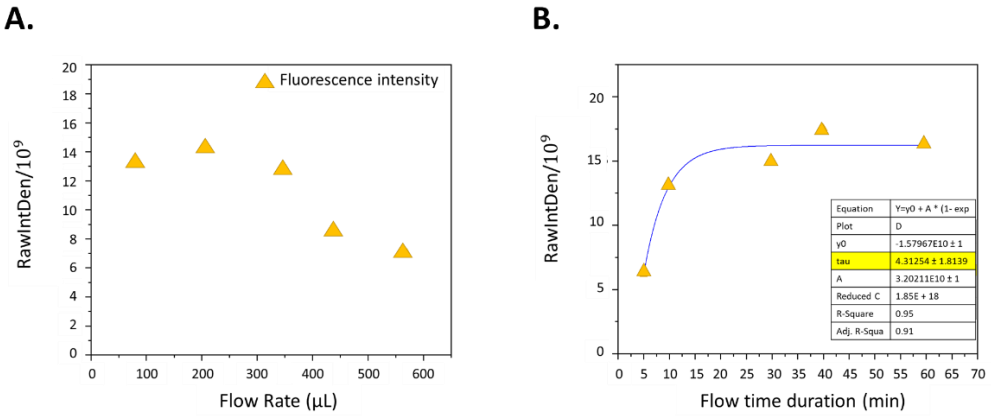

Figure 12. Kinetic study. The fluorescence intensity was evaluated firstly in function of flow rate **(A)**, then in function of flow time duration **(B)**. The kinetic study revealed that the highest fluorescence intensity is reached with a flow rate of ~220 µL/min and that 15 min are enough to obtain the optimal fluidic efficiency.

4.1.3 COMSOL flow simulation

The COMSOL Multiphysics suite has been used to accurately simulate the microfluidic device. Based on the finite element method, the software solves the Navier-Stokes equations discretizing the spatial domain in which the phenomenon occurs: the unknown variables are calculated in precise grid points and the other ones are derived through interpolations. A 3D cylindrical geometry was built and different materials – water in the domain, acrylic plastic for the cell's boundaries and gold on the bottom of the device to simulate the substrate - have been selected from the COMSOL material library. The Fluid Flow interface has been introduced to study the fluid behavior in the system.
The computed flows were calculated based on the assumption of a non-compressible fluid and with a no-slip boundary condition imposed on the wall domains. Since the Reynolds number is below a certain critical value, COMSOL's physics laminar flow with stationary study was used in simulation to compute physical quantities such as velocity and pressure fields. In addition, by coupling the Fluid Flow module with the Particle Tracing one, the study of particles' trajectories with certain density and size that flow within the fluid itself can be conducted allowing for detailed investigation of deposition, mixing and filtering devices.

4.1.4 Detection of biomarkers by reference methods

Before using the device for the detection of biomarkers of interest like HE4 and YKL-40 in serum samples, we measured their concentrations by two commercial standardized methods (reference methods), i.e., ELISA assay and Ella Protein-Simple system. Ella is a new generation system, based on microfluidics, which completely automates ELISAs using Simple Plex™ cartridge-based assays, thus reducing analysis time and technical errors.
Two serum pools were prepared by mixing 500µL of serum samples from 10 healthy adult males (pool A) and 10 healthy adult females (pool B). Firstly, we analyzed the calibration curve for both HE4 and YKL-40 assays in duplicate (Figure 13). The average ± SD of coefficient of variation (CV)% resulted equal to 1.98 ± 1.81 %.

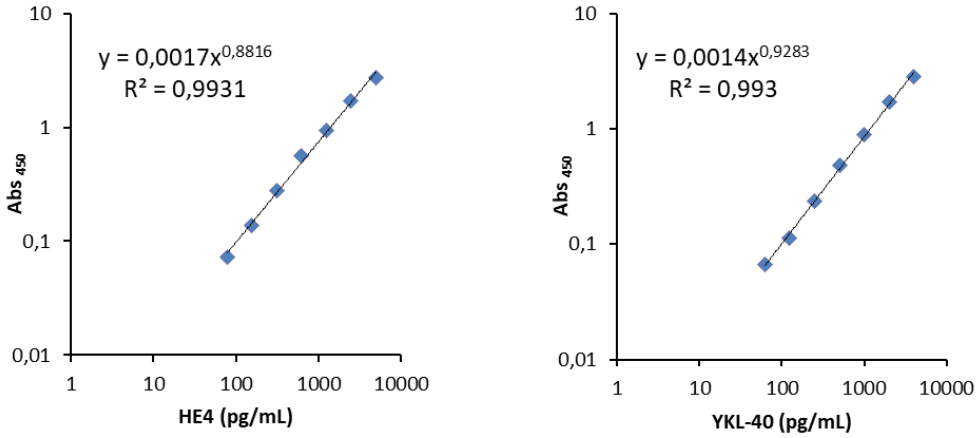

Figure 13. ELISA calibration curves of HE4 and YKL-40. The HE4 resulted linear in the range 78.1 – 5000 pg/mL. The YKL-40 resulted linear in the range 62.5 – 4000 pg/mL.

Then, the two pools were analyzed 8 times by both reference methods. The results are reported in Table 4.

Table 4. Biochemical analysis of serum HE4 and YKL-40 levels in the two serum pools.

	Pool A		**Pool B**	
	HE4 (pg/mL)	YKL-40 (pg/mL)	HE4 (pg/mL)	YKL-40 (pg/mL)
	Average (SE)		Average (SE)	
ELISA	6574 (62)	61730 (582)	5313 (42)	36271 (540)
ELLA	6253 (21)	60177 (648)	4099 (18)	27983 (389)
Average	6414	60954	4706	32127

4.1.5 Sensing Experiment

The Ab-functionalization of the nanostructure was accomplished through the well-established *photochemical immobilization technique* (PIT). An aqueous solution of mouse monoclonal anti-HE4 or anti-YKL-40 (500µL,

25 µg/mL) was irradiated by a Trylight® UV-lamp (Figure 14) for 30 s and flowed for 15 min onto the nanostructure by the above-mentioned microfluidic system.

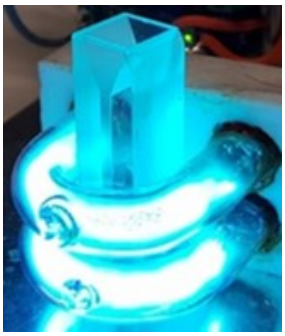

Figure 14. UV-lamp. The two U-shaped lamps allow the easy housing of standard 10mm quartz cuvette. The irradiation causes the photo-reduction of antibody disulfide bridges. The SH groups, so exposed, can guide the orientation of the antibody thanks to the covalent bond they establish with the surface.

Then, ultrapure water was flowed for 15 min to remove the unbound Abs and a BSA aqueous solution (500µL, 5 mg/mL) was flowed for 15 min to prevent non-specific adsorption. The desired amount of analyte was flowed onto the functionalized nanostructures for 15 min. According to the ELISA/Ella data, we used a 1/100 dilution serum sample for HE4 detection (~60 pg/ml of analyte) and 1/100 diluted serum sample for YKL-40 detection (~600 pg/ml of analyte). Later, ultrapure water was flowed for 15 min to remove the unbound analytes. A 500µL solution containing 2 µg/mL of FITC-labeled anti-HE4 or anti-YKL-40 was flowed for 15 min for the detection of the analyte of interest and, finally, ultrapure water was flowed for 15 min to remove the unbound antibodies.
At this point, the glass coverslip was moved from the microfluidic apparatus to the 24-multiwell customized mask to perform the measurement by microplate reader PHERAstar FSX. The measurement was performed using a fluorescence optical module with excitation at 485nm and emission at 520nm. Moreover, to increase the specificity of the assay, the reading of the region of interest was performed by scanning a 10x10 matrix and the peripheral pixels of the area were excluded to eliminate the fluorescence background of the mask plate. In this way, only the functionalized area of the slide was considered for the measurements.
Figure 15 shows the result of the PHERAstar FSX measurement where the fluorescence is expressed as color code (from a minimum of 5000 – in violet- to a maximum of 258884 – in red-). Additionally, the numerical values, expressed as fluorescence arbitrary unit (FU) are reported in Table 5.

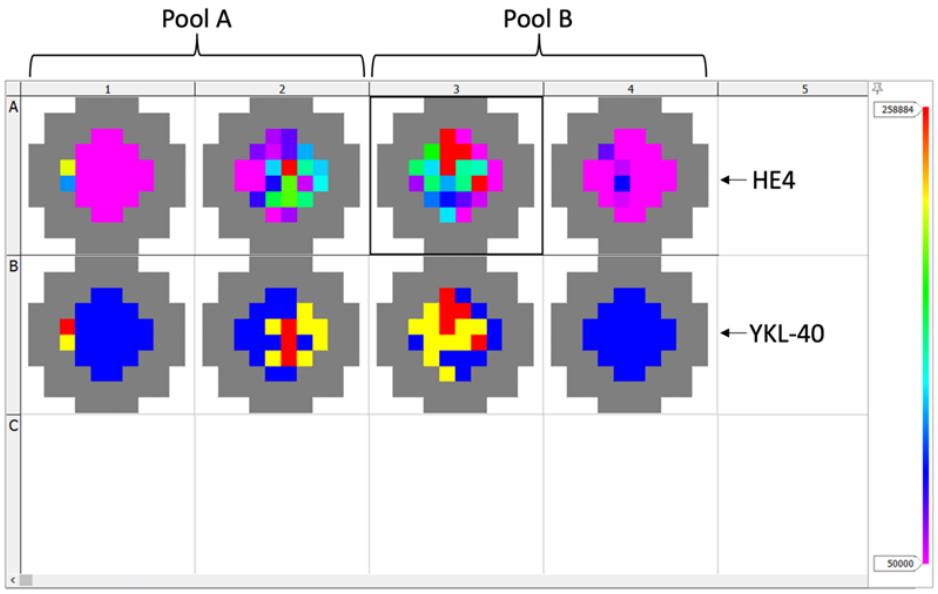

Figure 15. Output of PHERAstar FSX analysis. The fluorescence is expressed as color code. Each well corresponds to a slide used for the detection of HE4 or YKL-40 in a specific serum pool.

Table 5. PHERAstar FSX measurements.

		Antibody	**FU**
A1	Serum pool A	Anti-HE4	58183
A2	HE4-enriched serum Pool A	Anti-HE4	112920
A3	HE4-enriched serum Pool B	Anti-HE4	144665
A4	Serum pool B	Anti-HE4	52743
B1	Serum pool A	Anti-YKL-40	98183
B2	YKL-40-enriched serum Pool A	Anti-YKL-40	155420
B3	YKL-40-enriched serum Pool B	Anti-YKL-40	198665
B4	Serum pool B	Anti-YKL-40	87743

The detection of HE4 protein mirrors the concentrations measured by ELISA/Ella assays - samples A1 and A4 - with a good agreement also between samples A2 and A3, where the concentration of the HE4 protein was doubled enriched by adding the recombinant HE4 protein to serum pools.
Furthermore, we observed an increase in the basal signal in B1/B4 samples compared to A1/A4. Yet, this increase is lower than what we obtained from reference measurement methods. Indeed, according to ELISA data, the serum concentration of YKL-40 protein is 10-fold higher than HE4 one, whereas the PHERAstar ratio signal is just 1 to 2, from around 58000 to 98000 FU.

We observed a no-correspondence between ELISA/Ella assays and PHERAstar FSX analysis also for samples B1 and B4. According to reference methods, in fact, the serum concentration of YKL-40 in pool A (sample B1) is about twice that in pool B (sample B4), whereas the measurements obtained with PHERAstar FSX are comparable.

4.1.6 Molecular beacon design for miRNAs detection

Optical biosensors are versatile devices that can be used for the detection of different analytes. In the last two decades, miRNAs have emerged as powerful non-invasive diagnostic and prognostic biomarkers thanks to their accessibility, stability and specific expression pattern (Sohel, 2020). However, their low concentrations make their detection really challenging. Therefore, nanotechnology-based approaches represent a valid alternative to conventional detection methods. AuNPs have already been used in different miRNA sensors based, among others, on fluorescent and electrochemical detection (Coutinho and Somoza, 2019). We decided to exploit the fluorescent signal as we did for the protein detection. In this case, the gold-coated nanostructure surface will be functionalized with molecular beacons.
The structure of the molecular beacons, in fact, consists of a fluorophore (6-FAM) at 5' end, a loop sequence complementary to the target sequence, and a quencher (BHQ-1) at 3' end. Moreover, a thiol group was added at 3' to allow the covalent bond with the surface (Figure 16).

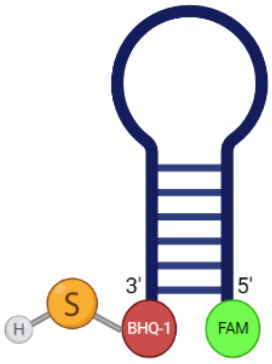

Figure 16. Molecular beacon structure. Molecular beacons are characterized by a loop sequence complementary to the target sequence, a fluorophore at 5' end a quencher at 3'. The thiol group is required to mediate the bond to AuNPs.

The schematic representation of miRNA detection strategy by gold-coated optical biosensor functionalized with molecular beacon is shown in Figure 17.

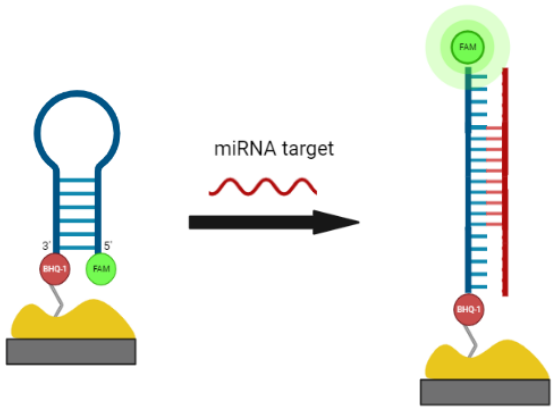

Figure 17. Representation of miRNA detection by optical biosensor. Optical biosensor based on gold-coated nanostructure surface will be functionalized with the molecular beacons. Upon the bond with the complementary sequence (miRNA target), the loop will open. The fluorophore will be distanced from the quencher, and this will lead to an increase of fluorescence intensity emission.

The synthesis of molecular beacons with a loop sequence complementary to miR-15b, miR-27a, miR-223 and miR-135b is currently in progress in the facility of C.E.I.N.G.E., Advanced Biotechnology.

4.2 Investigation of CIP2A role in cancer

Besides the role in diagnosis, biomarkers can be drug targets in the therapeutic approach. PP2A and especially CIP2A have been recently found to play a role in the carcinogenesis of EC, thus being considered as promising therapeutic targets for the treatment of this cancer.

4.2.1 Cellular model to investigate CIP2A role in cancer

According to *The Human Cancer Atlas*, CIP2A is recognized as an unfavorable prognostic marker in endometrial cancer. In order to investigate the effect of this protein on cell proliferation, cell metabolism and drug sensitivity, we first down-regulated its expression by shRNA lentivirus infection.

However, in absence of an endometrial cellular model, we used for this study leukemic cell lines (K562 and Kasumi), where CIP2A was found overexpressed (Chen, 2011).
As shown in Figure 18A and 18C we obtained a good *knock-down* efficiency at mRNA and protein levels in K562 cell line. Although in Kasumi cells we were not able to observe the down-regulation of CIP2A at mRNA level (Figure 18B), the amount of protein is significantly decreased in Kasumi-shCIP2A cells compared to Kasumi shScramble (Figure 18D). Additionally, CIP2A KD in Kasumi cells results in a decrease in the protein amount of c-Myc as well as in the ratio between phospho-c-Myc-S62 and total c-Myc (Figure 18E). This result is in line with the role CIP2A plays in Myc stabilization (Westermarck, 2007).

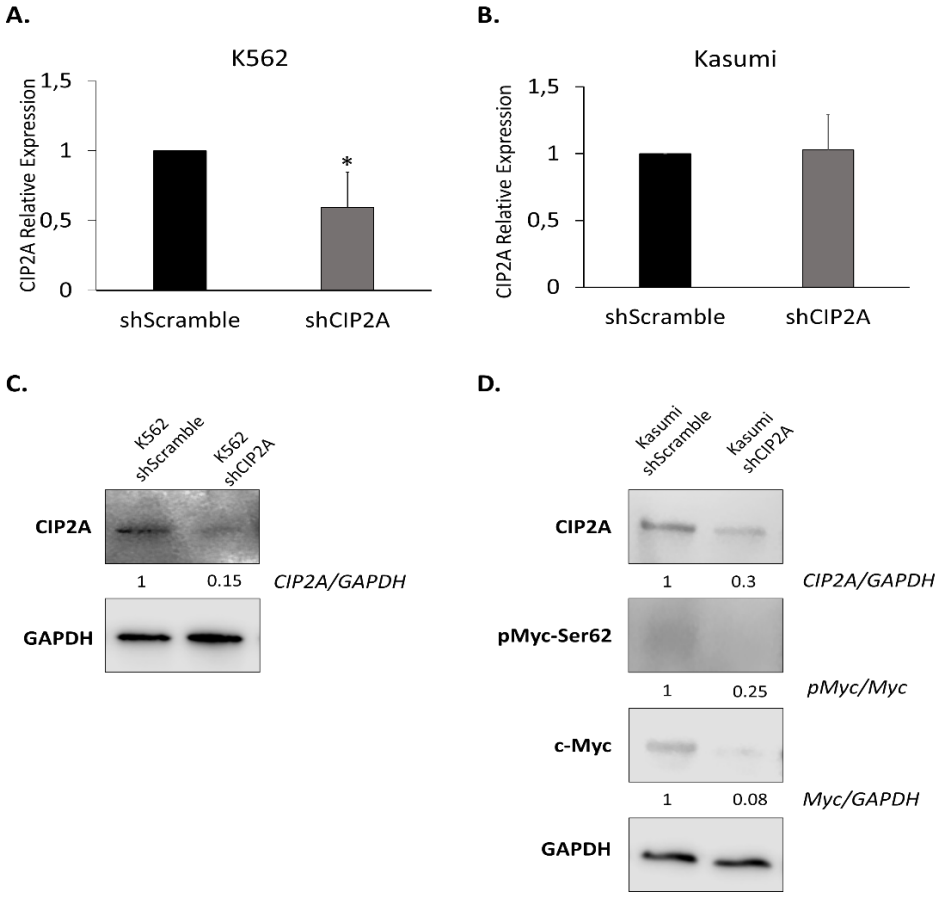

Figure 18. Knock-down of CIP2A at mRNA (A/B) and protein (C/D) level. In K562 cell line a good *knock-down* of CIP2A was observed both at mRNA **(A)** and protein **(C)** level. In Kasumi, no *knock-down* was observed at mRNA level **(B)**, but the amount of protein was significantly decreased in Kasumi-shCIP2A cells compared to Kasumi-shScramble **(D)**. mRNA and protein expression levels were normalized with GAPDH. In Kasumi cells, the CIP2A KD also decreased the protein amount of c-Myc as well as the ratio between phospho-c-Myc-S62 and total c-Myc **(D)**.
CIP2A relative expression was calculated using the Pfaffl formula. For each cell line shCIP2A was compared to shScramble, set equal to 1. t-test; *$p<0,05$.

4.2.2 CIP2A is essential for self-renewal

We checked the effect of CIP2A on self-renewal ability through colony-formation assay. After shRNA infection, K562 cells were cultured in the MethoCult medium and re-plated for three times. The results showed a significant reduction in colony number at the third round in cells infected with shCIP2A compared to shScramble (Figure 19A). Furthermore, it seemed to be a difference also in the morphology of colonies. In particular, in the first and second round, when the size of the colonies was smaller, we could see that shCIP2A cells created scattered colonies, instead of compact ones (Figure 19B).

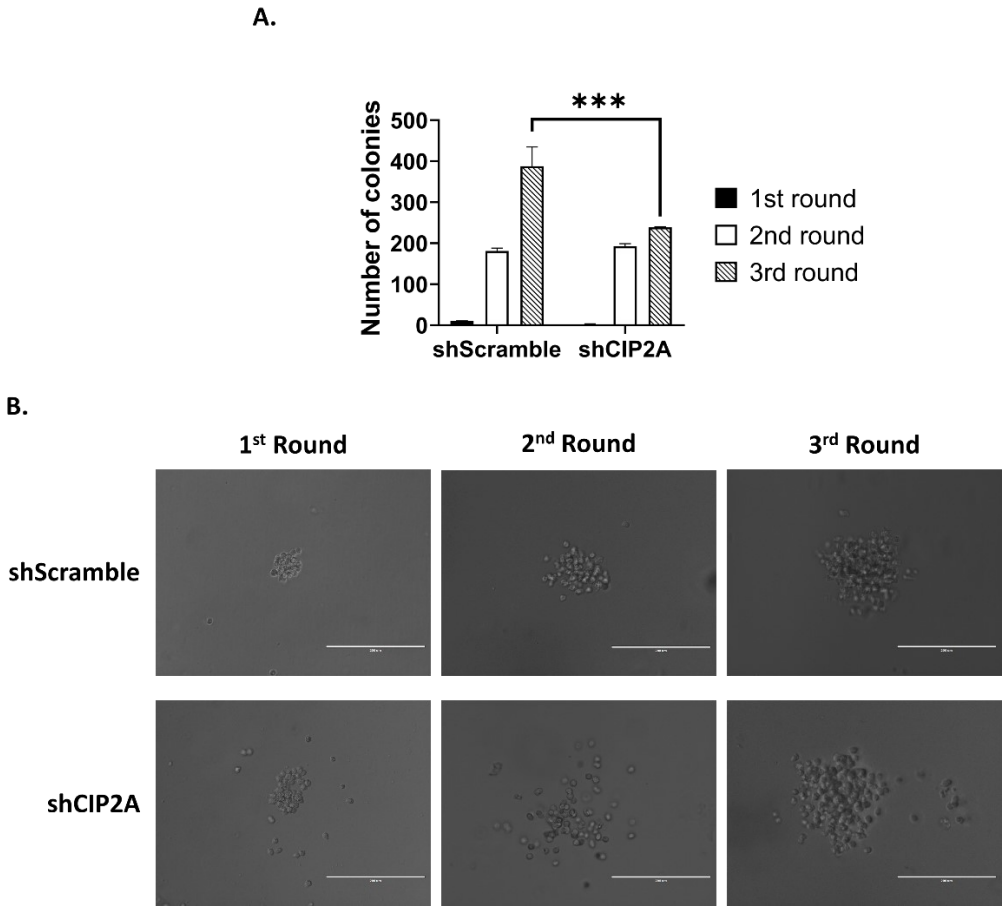

Figure 19. Effect of CIP2A KD on K562 Colony - Forming Unit ability. A) Colony number. A significant decrease in the number of colonies was observed in K562-shCIP2A compared to K562-shScramble. ****p<0,001*. **B) Colony morphology.** K562-shCIP2A colonies appear less compact than K562-shScramble colonies. Images were captured using EVOS™ cell image system (magnification 40X) and are representative of 3 rounds puromycin selection.

4.2.3 CIP2A depletion effect on cell proliferation

The effect of CIP2A depletion on cell proliferation was evaluated both in K562 and Kasumi cells. Interestingly, we observed a different behavior in the two cell lines. Whilst the K562-shCIP2A cells showed a significant decrease in proliferation rate when compared to K562-shScramble, what we saw in Kasumi cells was the opposite (Figure 20).

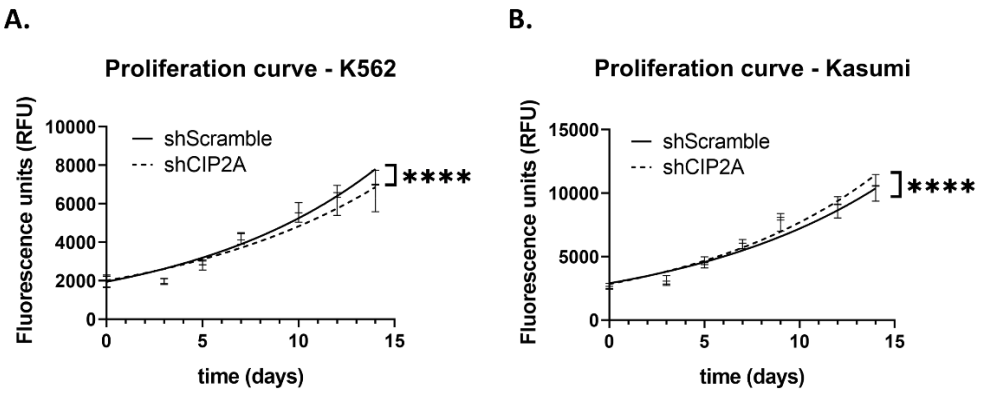

Figure 20. CIP2A depletion effect on cell proliferation in K562 (A) and Kasumi (B). GFP autofluorescence was used as a quantitative reporter of cell proliferation. For each cell line, the same number of cells was plated at T0 and the GFP signal was measured with a fluorescent microplate reader. Data shown as mean ± SD of triplicate wells and are representative of two independent experiments. 2-way ANOVA test was performed between shScramble - shCIP2A at the 14th day. ****$p<0,0001$.

4.2.4 CIP2A could be involved in the response to oxidative stress

Considering the different effect that the depletion of CIP2A has on cell proliferation in the two cell lines used in this study, we wondered if CIP2A could be involved in the response to oxidative stress and DNA damage. To figure out it, we treated Kasumi-shScramble and Kasumi-shCIP2A with the anthracycline Daunorubicin. This drug is used in the treatment of acute myeloid leukemia and acute lymphoblastic leukemia and possess multiple mechanisms of actions (Laurent and Jaffrézou, 2001). Daunorubicin binds the sugar-phosphate backbone of DNA, thus inhibiting Topoisomerase II, an enzyme needed to unwind DNA for transcription. This leads to the formation of DNA double strand breaks (DSBs). In addition, Daunorubicin is metabolized by cytochrome P450 reductase resulting in the formation of free radicals (ROS) that can damage bases of DNA (oxidation), creating single strand breaks (SSBs). The overall effect is cell cycle arrest and cell death.
Firstly, we treated Kasumi-shScramble and Kasumi-shCIP2A with Daunorubicin for 72h to evaluate the effect of distinct drug concentrations

(10nM, 25nM and 50nM) on cell viability (Figure 21). However, after 72h the percentage of dead cells was too high (between 40% and 50% with 25nM of Daunorubicin, between 70% and 85% with 50nM), so we decided to reduce the treatment to 48h to evaluate the accumulation of oxidative stress.

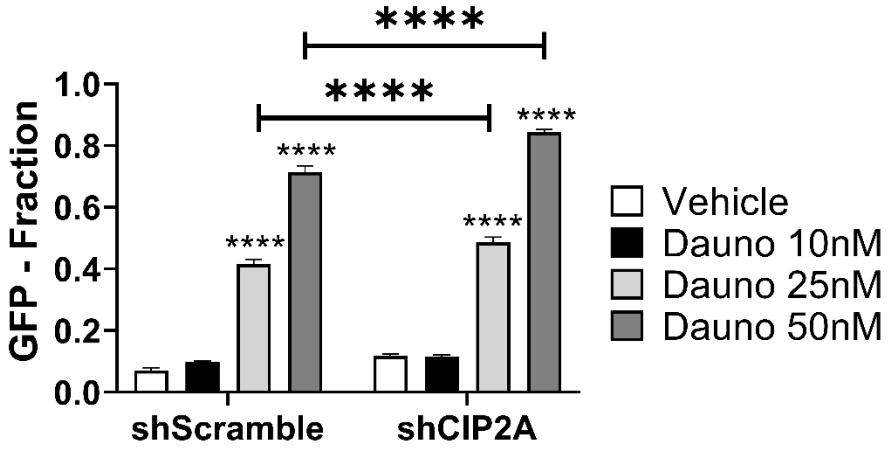

Figure 21. Analysis of cell death in Kasumi cells after 72h of Daunorubicin (Dauno) treatment. The fraction of Kasumi dead cells (GFP -) increases with higher doses of Daunorubicin (*****p<0,0001*). A significant increase in cell death was observed at 25nM and 50nM (*****p<0,0001*) when shCIP2A was compared to shScramble. GFP was used as viability reporter. Data shown as mean ± SD of triplicate wells. 2-way ANOVA test was performed between vehicle vs Dauno 10nM / 25nM / 50nM for each cell line, shScramble - shCIP2A for each treatment.

This time not only Kasumi-shScramble and Kasumi-shCIP2A, but also K562-shScramble and K562-shCIP2A cells were treated. After 48h we evaluated both cell death and cellular oxidative stress levels through CellRox signal.
We observed an increase in cell death in cells treated with Daunorubicin, but there was a significant difference between shScramble and shCIP2A clones only at 50nM (Figure 22A/C). Furthermore, we measured the oxidative stress levels, expressed as Median Fluorescence Intensity (MFI), in alive cells. Considering that the percentage of cells surviving from treatment with 50nM of Daunorubicin was still too low, we decided to exclude the results of oxidative stress related to this concentration as they would not be representative of the effect we wanted to evaluate. Interestingly, we saw a significant increase of oxidative stress in treated cells, both K562 and Kasumi: the oxidative stress levels were almost tripled in cells treated with 25nM of Daunorubicin compared to the vehicle. Nevertheless, there was no difference between shScramble and shCIP2A clones (Figure 22B/D).

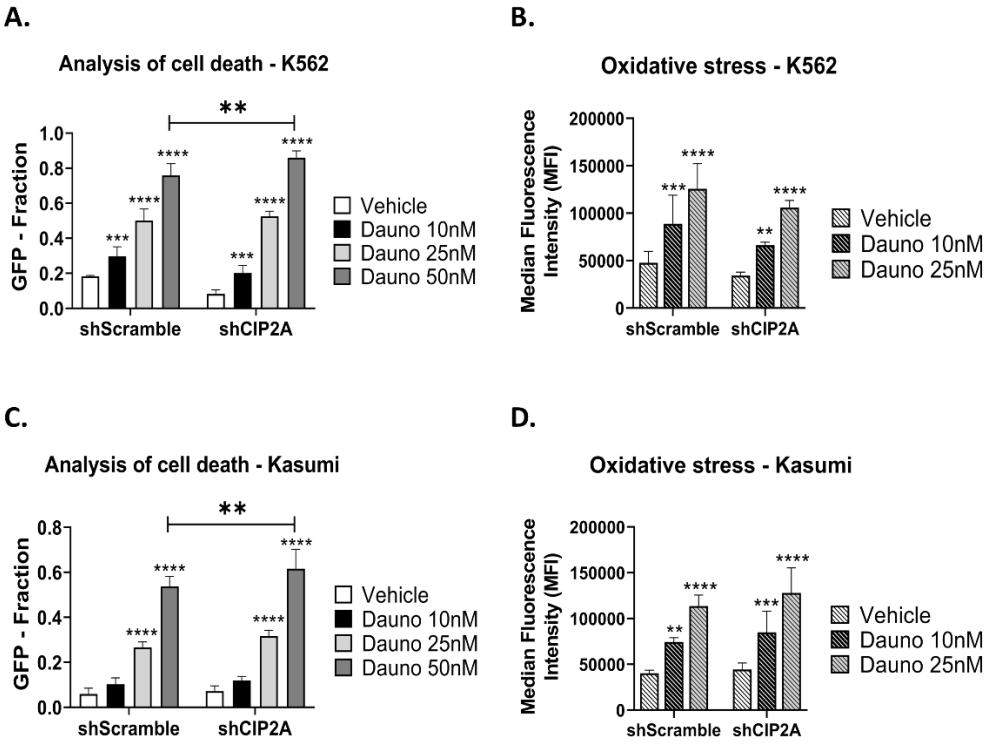

Figure 22. Analysis of cell death in K562 (A) and Kasumi (C) cells upon Daunorubicin treatment. The fraction of K562 and Kasumi dead cells (GFP -) increases with higher doses of Dauno (****p<0,001; ******p<0,0001*). A significant increase in cell death was observed at 50nM (***p<0,01*) in both cell lines when shCIP2A was compared to shScramble. **Oxidative stress levels in K562 (B) and Kasumi (D) cells.** The oxidative stress levels, expressed as MFI, increase upon the treatment with 10nM and 25nM of Dauno compared to the vehicle, but no significant difference was observed between shScramble and shCIP2A neither in K562 nor in Kasumi cell lines. Data shown as mean ± SD of triplicate wells and are representative of two independent experiments. 2-way ANOVA test was performed between vehicle vs Dauno 10nM / 25nM / 50nM for each cell line, shScramble - shCIP2A for each treatment.

Finally, we treated Kasumi-shScramble and Kasumi-shCIP2A with 25nM of Daunorubicin for 24h to analyze the DNA damage by immunofluorescence, using γH2AX as marker (Almasan, 2012; Esposito and So, 2014). As expected, we could detect a high number of γH2AX foci in Kasumi-shScramble when treated with Daunorubicin compared to cells treated with the vehicle. On the contrary, no DNA damage was observed in Kasumi-shCIP2A upon Daunorubicin treatment (Figure 23).

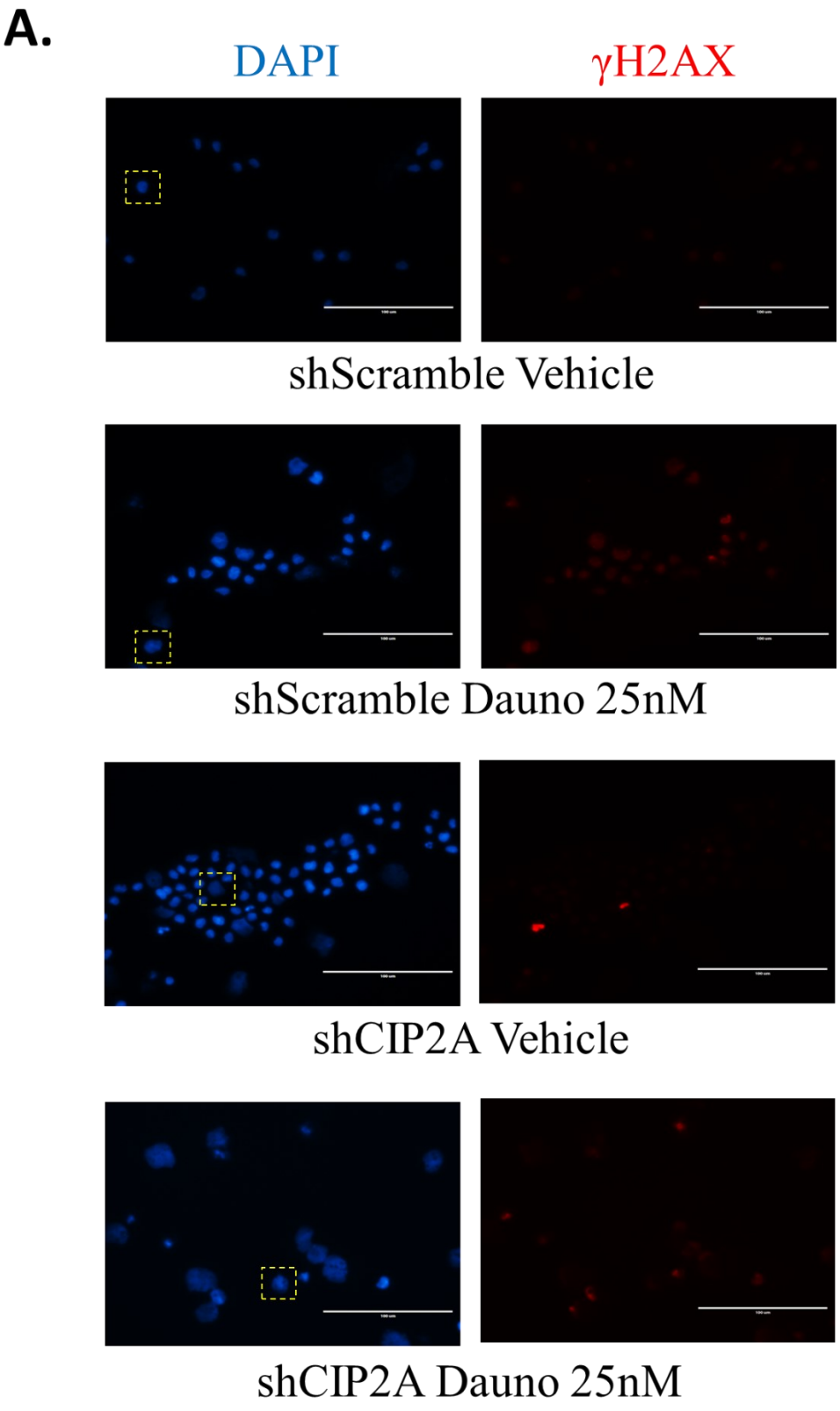
A.
DAPI
γH2AX
shScramble Vehicle
shScramble Dauno 25nM
shCIP2A Vehicle
shCIP2A Dauno 25nM

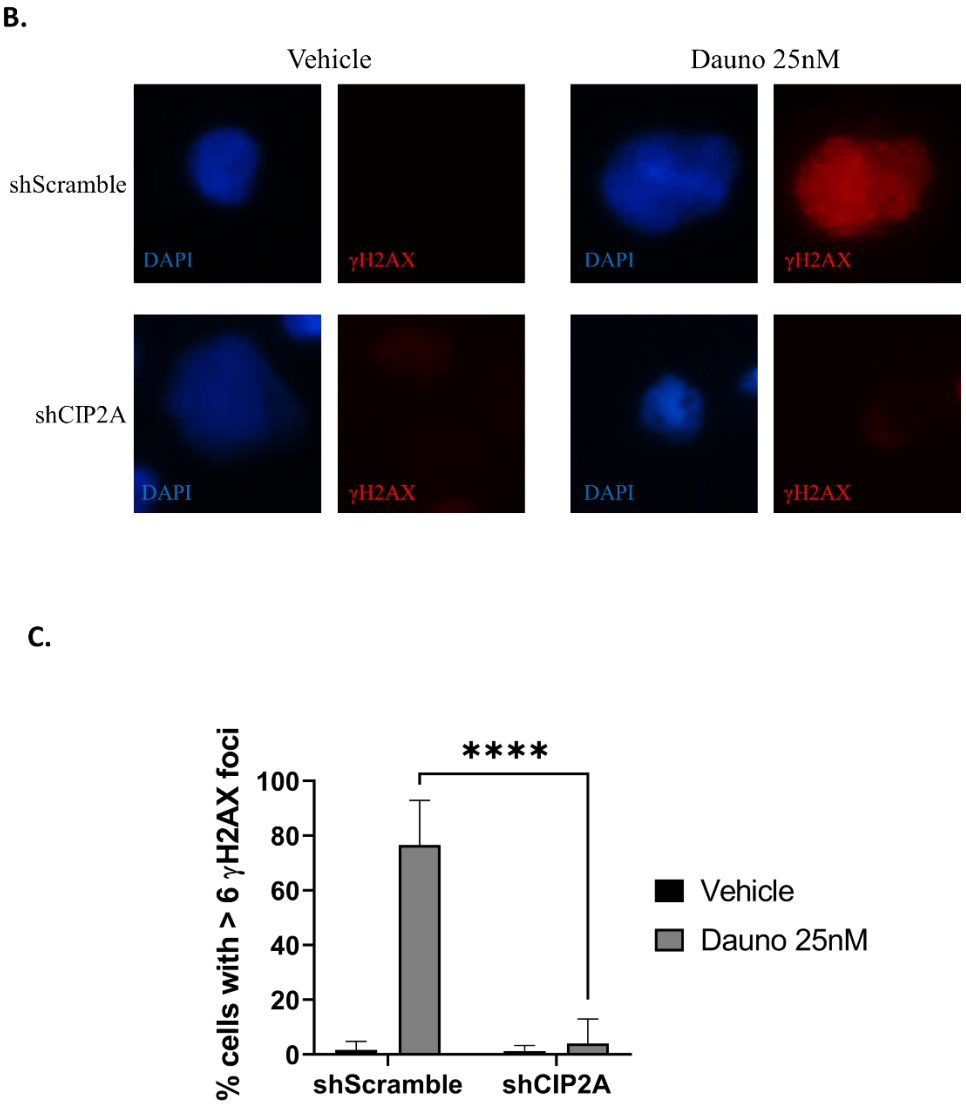

Figure 23. Analysis of DNA damage by Immunofluorescence. A) Representative images of each cell line and condition analyzed. Kasumi-shScramble showed a significant accumulation of DNA damage (red signal) upon Daunorubicin treatment. On the contrary, no difference was observed in Kasumi-shCIP2A between cells treated with vehicle and Daunorubicin. Images were captured using EVOS™ cell image system (magnification 40X). **B) Magnification of a selected nucleus from each of the field above.** The selected nuclei are highlighted by the yellow boxes in point A. **C) Histogram of DNA damage analysis.** The percentage of cells with DNA damage is drastically reduced in Kasumi-shCIP2A compared to Kasumi-shScramble. 2-way ANOVA test was performed between shScramble - shCIP2A. ****$p<0,0001$.

4.2.5 Carfilzomib affect the expression of CIP2A in K562 cell line

CIP2A controls the stability of Myc, a key oncoprotein. This evidence has led to hypothesize that targeting CIP2A could be a promising therapeutic strategy. However, there are no specific CIP2A inhibitors that can be tested. Carfilzomib has been identified as a drug able to regulate CIP2A at transcriptional level (Chen, 2017a), we therefore tested whether CIP2A KD sensitizes the leukemic cells to Carfilzomib. Firstly, K562 and Kasumi cells were treated with 10nM of Carfilzomib. The concentration of the drug to be used was chosen based on previous experiments performed by Dr. Maria Teresa Esposito in order to have an effect on the cells, without killing all of them. After 48h of treatment, cells were collected and analyzed for qRT-PCR. The results showed a significant decrease in mRNA levels of CIP2A only in K562 cells (Figure 24).

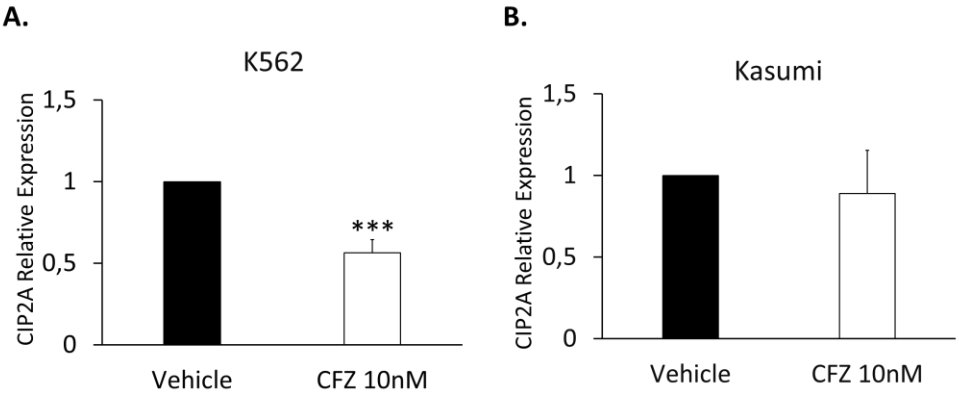

Figure 24. CIP2A expression upon Carfilzomib treatment in K562 (A) and Kasumi (B) cells. qRT-PCR performed on cells treated with vehicle and 10nM of Carfilzomib. CIP2A relative expression was calculated using the Pfaffl formula. *GAPDH* was used as housekeeping for the normalization. For each cell line CFZ 10nM was compared to Vehicle, set equal to 1. t-test; ***p<0,001.

4.2.6 CIP2A down-regulation increases cell sensitivity to Carfilzomib

Finally, we checked whether CIP2A influences the cell sensitivity to Carfilzomib. K562-shScramble, K562-shCIP2A, Kasumi-shScramble and Kasumi-shCIP2A cells were treated for 72h with three different concentration of Carfilzomib (5nM, 10nM and 20nM) and then the cell death was evaluated by FACS.

The fraction of K562 and Kasumi dead cells increases with higher doses of Carfilzomib, thus confirming the sensitivity of these cell lines to the drug. Moreover, we could see a significant increase in cell mortality in K562-shCIP2A compared to K562-shScramble, both at 10nM and 20nM of Carfilzomib (Figure25A). On the contrary, by comparing Kasumi-shCIP2A and Kasumi-shScramble, a significant increase of cell death was only observed when cells were treated with 20nM of Carfilzomib (Figure 25B).

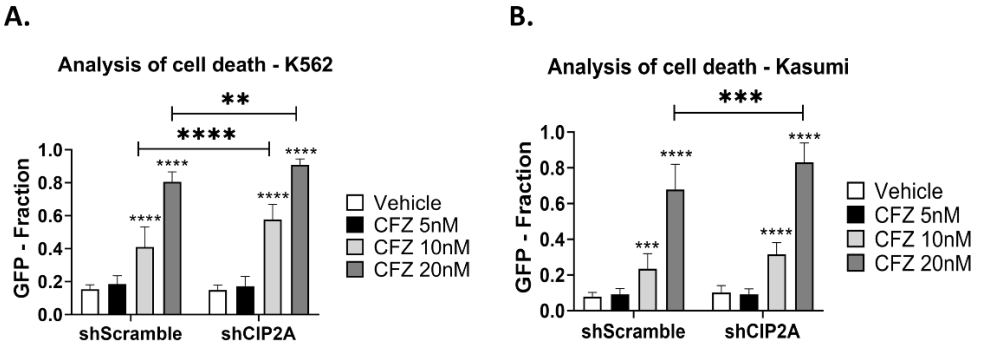

Figure 25. Effect of Carfilzomib (CFZ) on cell death in K562 (A) and Kasumi (B). The fraction of K562 and Kasumi dead cells (GFP -) increases with higher doses of CFZ (****p<0,001; ****p<0,0001*). A significant increase in cell death at 10nM (****p<0,0001*) and 20nM *(**p<0,01*) of CFZ was observed in K562 when shCIP2A was compared to shScramble. Additionally, a significant increase in cell death was observed in Kasumi-shCIP2A compared to Kasumi-shScramble, but only when cells were treated with 20nM of CFZ (****p<0,001*). Data shown as mean ± SD of triplicate wells and are representative of three independent experiments. 2-way ANOVA test was performed between vehicle vs CFZ 5nM / 10nM / 20nM for each cell line, shScramble - shCIP2A for each treatment.

5. DISCUSSION

The incidence and the mortality rate of endometrial cancer has rapidly increased in last years and now EC represents the 6th most common malignancy worldwide (Zhang, 2021).
Despite the high frequency of EC and the intense research on this topic, few are the progress made so far both for the diagnosis and therapy of this cancer.
Currently, the diagnosis is based on invasive and painful tests which are carried out in presence of symptoms like abnormal vaginal bleeding. Although this symptom is found in ~90% of patients with EC, only 9% of women with post-menopausal bleeding is diagnosed with endometrial cancer (Wentzensen, 2018). This emphasizes the need for alternative diagnostic tests that are more specific and based on less invasive methodologies. Recently, Wang *et al.* developed a new test, called PapSEEK, which is able to detect mutations in some of the genes commonly mutated in EC (Papadopoulos, 2018). This multiplex PCR-based test analyzes DNA obtained from the fluids collected during a routine Pap test. Although promising, this study has several limitations, among which the low sensitivity (alterations were identified in more women with late-stage than early-stage) and the fact that only samples from patients with a known diagnosis of cancer were examined.
In light of this, researchers are still trying to develop a screening test that could allow the early diagnosis of EC even in women without any symptoms. Therefore, there is a growing interest in identifying tumor markers whose altered expression in blood or other non-invasive biological samples can be used with a diagnostic or prognostic purpose and may help in driving the choice of the therapeutic approach.
Many biomolecules have been identified so far as putative biomarkers for EC, including metabolites, individual proteins and panels of proteins, and miRNAs. Troisi *et al.*, for instance, developed and validated a serum metabolomic signature for EC screening in post-menopausal women. They showed that the blood levels of lactic acid, homocysteine and hydroxybutyrate are increased in patients compared to controls, whereas other metabolites like linoleic acid, stearic acid and myristic acid are decreased (Guida, 2018; Guida, 2020).
Among the proteins, CA-125 and HE4 are the most widely studied. Several studies have investigated the diagnostic potential of HE4 in comparison to CA-125 and in all of them HE4 displayed a higher sensitivity and specificity in distinguishing between patients with EC and healthy women. (Ravaggi, 2012; Benedetti-Panici, 2013; Høgdall, 2013; de Leon-Luis, 2021). HE4 might be also a useful prognostic marker in EC, given to the correlation between its levels and histopathological factors as myometrial invasion, stage, tumor size and lymph node metastases (Panyavaranant and Manchana, 2020; Van de Vijver, 2017; Baquedano Mainar, 2020).
Thanks to these encouraging results, many combinations of HE4 with other markers have been investigated and the most effective one seems to be

HE4+EpCAM panel which showed a sensitivity of 93% and an AUC value of 0,87 (Ma, 2020). Benati *et al.* reached an AUC of 0,96 by combining HE4 with DJ-1, but no sensitivity and specificity values were reported in their study (Lippi, 2018). YKL-40 has also been studied as individual protein, showing a good diagnostic accuracy in detecting EC (He, 2014).

In the last two decades, miRNAs have emerged as powerful non-invasive diagnostic and prognostic biomarkers thanks to their accessibility, stability and specific expression pattern (Sohel, 2020). Although it is possible to distinguish miRNAs acting as oncogenes or onco-suppressors, the distinction is not always so clear. As a matter of fact, some miRNAs can mediate opposite effects in different types of cancer. A variety of miRNAs have been found de-regulated in EC like miR-15b, miR-27a, miR-223 and miR-135b (Tu, 2014; Abouzeid, 2021; Xiang, 2013; Masuzaki, 2014).

Despite such evidence, the results on the sensitivity of these biomarkers are very variable due to the heterogeneity in the *cut-off* value used, the small cohort of subjects analyzed and the use of different control groups. Furthermore, it is really unlikely to find a tumor marker that could fulfils all the criteria of sensitivity and specificity required, so the combinations of different biomarkers would be a better choice not only to improve the accuracy in identifying EC, but also to distinguish it from other pathological conditions. The detection method is another important aspect to consider. In the clinical routine a cheap, sensitive, easy-to-use and fast-response methodology would allow rapid and reliable analyses even in poorly equipped laboratories.

Therefore, the present study reinforces the already widespread idea about the great potential of biosensors as detection methods. Indeed, optical biosensors have a high sensitivity and multiplexing analysis ability which enable them to detect very low quantities of multiple analytes simultaneously.

Our project has been carried out in collaboration with the Department of Physics "Ettore Pancini" of the University of Naples Federico II. In last years, Velotta and his team developed a technique to immobilize antibodies on surfaces reactive to thiols (e.g., gold). This *Photochemical Immobilization Technique* (PIT) is based on the photo-reduction of antibody disulfide bridges by UV radiation. The SH groups, so exposed, can guide the orientation of the antibody thanks to the covalent bond they establish with the surface (Velotta, 2019a). PIT was successfully used to functionalize nanostructured surfaces, exploiting the phenomenon of MEF, to detect IgG in urine samples at very low concentrations (<10µg/L) (Velotta, 2019b). Based on these results, the present study has proposed to develop and functionalize these biosensors for the detection of endometrial tumor markers.

A preliminary kinetic study, in which solutions of IgG were flowed onto the nanostructure, revealed that a flow rate of ~220 µL/min and a flow time duration of 15 min ensure the optimal fluidic efficiency. With this flow rate setting, we functionalized the nanostructure surfaces with specific antibodies to detect proteins, identified as good diagnostic biomarkers for the EC, in serum samples. We prepared two serum pools by mixing serum samples from 10

healthy adult males (pool A) and 10 healthy adult females (pool B), to test our biosensor with a real biological sample. Firstly, we accurately evaluated the concentration levels of HE4 and YKL-40 proteins in the two serum pools by two reference methods, ELISA assay and Ella Protein-Simple system. Later, we detected the levels of these two proteins by using the biosensor developed. In this case, we measured HE4 and YKL-40 levels not only in the two serum pools used by mixing serum samples from healthy subjects, but also in the same pools where the concentration of the two proteins was enriched by adding recombinant proteins in order to mimic the pathological condition. The preliminary test revealed that the biosensor is able to discriminate the physiological range values from pathological ones both for HE4 and YKL-40. Additionally, we observed a great correspondence with ELISA and Ella systems in terms of concentration ratio for HE4 protein. On the contrary, the difference we observed in serum concentration of YKL-40 in the two pools by ELISA/Ella assays was not reflected by detection with the biosensor.

Although these preliminary data need to be repeated and the system has to be validated with a dose-response curve to evaluate its sensitivity and specificity, the aim of this part of the project was to develop a point-of-care screening system, able of discriminating between normal and pathological values. In fact, ease of use and fast-response analyses make optical biosensors powerful tools that would be well suited for first level screening. Considering that prognosis and therapeutic approach are strongly linked to early diagnosis, it is crucial to have a first level screening to identify putative subjects with altered cancer biomarker levels which will be later validated by a second level screening based on reference assays.

Besides their role in diagnosis, tumor markers may also play a role in the choice of therapeutic treatment. To date, the standard treatment for EC is surgery and adjuvant therapy, including radiotherapy, chemotherapy and hormone therapy. Furthermore, the molecular classification of EC has led to the identification of potential therapeutic targets, thus paving the way to a personalized treatment. For instance, some checkpoint inhibitors showed to be effective in patients with the MMR-d subtype (Diaz, 2020; Australia New Zealand Gynaecological Oncology Group (ANZGOG), 2021). mTOR inhibitors have been investigated for their low toxicity, but they showed a modest effect when used alone. A slight improvement can be reached in combination therapies (Slomovitz and Coleman, 2012; Ferrero, 2019*).*

In this scenario, PP2A is emerging, among others, as novel therapeutic target. Its inactivation is observed in both types of EC, albeit through different mechanisms (Remmerie and Janssens, 2019). In the most frequent type I EC, PP2A is inactivated by the over-expression of one of its main inhibitors, CIP2A. The mechanism underlying the over-expression of CIP2A is still unknown, yet estradiol has been proven to increase CIP2A protein levels through the estrogen receptor α (ERα) in ER-positive breast cancer (Yang, 2014). This could also be true for type I EC, which is estrogen-dependent, and explain why the over-expression of CIP2A seldom occurs in type II EC.

Few studies have reported that CIP2A is up-regulated in patients with EC and that its levels correlate with a worse prognosis (Akgün, 2020; Zhang, 2017*)*. Therefore, we wanted to investigate its biological function by evaluating the effect of this protein on cell proliferation, cell metabolism and drug sensitivity. Considering that the role CIP2A plays in cancer needs to be further elucidated, the model we used for this study is represented by leukemic cell lines, where this protein was found significantly over-expressed (Chen, 2011). In particular, we used a chronic leukemia cell model (K562) and an acute leukemia cell model (Kasumi). We found that the depletion of CIP2A decreases the protein amount of c-Myc as well as its SER62 phosphorylated form in Kasumi cells and this is in line with the role CIP2A has in phospho-c-Myc stabilization (Westermarck, 2007). Peng *et al.* showed that the *knock-down* of CIP2A even decreases the expression of several proteins belonging to metabolism, like glycolytic enzymes, and of Glutathione S Transferase (GST), which plays a key role in the detoxification and drug resistance, thereby decreasing the cell proliferation rate (Zhang, 2015). While we could observe a decrease in proliferation in K562-shCIP2A, interestingly, the Kasumi-shCIP2A cells showed an unexpected increase in cell growth. According to a preliminary metabolomic analysis, in comparison with the shScramble cells in these Kasumi-shCIP2A cells there is a lower amount of glucose-6-Phosphate, an intermediate of the glycolytic pathway, which is also a precursor of the PPP pathway that feeds into synthesis of nucleotides. Therefore, a reduction in glucose-6-Phosphate in Kasumi-shCIP2A cells might indicate a higher consumption of this metabolite to meet the metabolic demand of faster growth rate and support the increased proliferation (Patra and Hay, 2014; Wu, 2014). The metabolomic analysis also showed in Kasumi-shCIP2A cells a shift to oxidative phosphorylation, which, combined to a decrease in GST, could lead to accumulation of oxidative stress. We therefore decided to evaluate the ability of these cells to respond to drugs that induce oxidative stress, such as Daunorubicin. We observed that in both K562 and Kasumi the CIP2A KD increased the response only to 50nM Daunorubicin. No statistically significant difference was reported for concentrations of 10-25nM. Moreover, at these concentrations, we could not detect any significant difference between shScramble and shCIP2A clones in the oxidative stress accumulated upon Daunorubicin treatment. Instead, when we analyzed the DNA damage accumulation upon Daunorubicin treatment by γH2AX staining, we detected DNA damage only in the shScramble controls, but not in the shCIP2A cells. This result might seem in contrast with the oxidative stress data. Daunorubicin inhibits the action of Topoisomerase II by binding the sugar-phosphate backbone of DNA and thereby causing the formation of DSBs. This leads to the formation of γH2AX foci to recruit DNA repair proteins (Kuo and Yang, 2008). Although we did not detect γH2AX in Kasumi-shCIP2A treated with Daunorubicin, this might be due to a lack of phosphorylation of the histone protein H2AX rather than an effective absence of DNA damage. In fact, H2AX is phosphorylated by kinases like ataxia telangiectasia mutated (ATM) and

ATM-Rad3-related (ATR) in the PI3K pathway which includes proteins frequently mutated in cancer and that are downstream targets of PP2A.
As for K562 cell line, we were unable to evaluate the amount of c-Myc in these cells because of technical issues (the signal of this protein is very weak and difficult to detect). However, previous data obtained by Dr. Maria Teresa Esposito showed that the CIP2A KD results in an increased degradation of c-Myc in K562 as well. In support of this, in fact, cell proliferation was inhibited in K562-shCIP2A cells. This is probably due to the down-regulation of c-Myc which is the master regulator of cellular proliferation (Sedoris, 2012). Additionally, our results showed that CIP2A plays an important role also in the self-renewal ability of these cells, since its depletion affects the capability of K562 to form colonies in semi-solid medium.
The last step of our study was represented by the investigation of CIP2A role in drug sensitivity. Several studies have shown that the overexpression of CIP2A is correlated to drug resistance because of the up-regulation of the P-glycoprotein drug efflux pump mediated by CIP2A (Yang, 2011; Wang, 2016; Wang, 2019). Additionally, CIP2A controls the stability of c-Myc and this evidence has led to hypothesize that targeting CIP2A could be a promising therapeutic strategy. However, there are no specific CIP2A inhibitors that can be tested. Carfilzomib has been identified as a drug able to regulate CIP2A at transcriptional level via disrupting the interaction between its promotor and the transcription factor Elk1 (Chen, 2017). Therefore, we tested whether CIP2A KD sensitizes the leukemic cells to Carfilzomib.
Firstly, we treated the untrasduced K562 and Kasumi with 10nM of this drug and checked the mRNA levels of CIP2A after 48h. We could only find a down-regulation of CIP2A in K562, and this result is in contrast to literature data. Liu *et al.*, in fact, achieved an excellent down-regulation of CIP2A following treatment with very high doses of Carfilzomib – up to 200nM – in different leukemic cell lines (HL-60, KG-1 and THP1), but not in K562 (Chen, 2017). In addition, we evaluated the cell response to Carfilzomib and found that the depletion of CIP2A increases cell sensitivity to this drug in both chronic and acute leukemia cell lines, thus supporting the involvement of CIP2A in drug resistance. Nevertheless, Kasumi cells seems to be less sensitive compared to K562 cells – a significant increase in cell death was observed only when Kasumi-shCIP2A cells were treated with 20nM of Carfilzomib.
In conclusion, even if there are still gaps that need to be filled, these results suggest that CIP2A could be a good therapeutic target and it is worth to deeply investigate its role in different types of cancer. Moreover, the inhibition of CIP2A could not only have a direct anti-tumorigenic effect, but also rescue the activity of PP2A which is crucial in many signaling pathways.
With regard to EC, *Yu et al.* had already showed that CIP2A depletion inhibits cell proliferation and invasion and increases apoptosis (Zhang, 2018). Consequently, it would be interesting to test whether the down-regulation of CIP2A would have an effect on cell sensitivity to drugs like Carfilzomib also in an endometrial cell model.

6. CONCLUSIONS

In this study, we developed optical biosensors, based on *Metal Enhanced Fluorescence* (MEF) technology, to detect serum diagnostic biomarkers of EC. Although additional tests are required to validate the system and to evaluate its sensitivity and specificity, our preliminary data show the great potential of these devices. Thanks to the ease of use and fast-response analysis, optical biosensors represent a valid method as a point-of-care screening system to distinguish a biological condition from a pathological one.
We also investigated the role of CIP2A as therapeutic biomarker. In particular, we reported that the depletion of CIP2A affects the self-renewal ability of K562 cells, which showed a decreased capability to form colonies in semi-solid medium. Furthermore, the CIP2A KD can sensitize the leukemic cells to the proteasome inhibitor Carfilzomib. Although our findings need to be demonstrated in an endometrial cell model, they suggest that the inhibition of CIP2A might be a valid therapeutic option in cancer treatment.

7. LIST OF PUBLICATIONS

Berni Canani R, Comegna M, Paparo L, Cernera G, Bruno C, Strisciuglio C, **Zollo I**, Gravina AG, Miele E, Cantone E, Gennarelli N, Nocerino R, Carucci L, Giglio V, Amato F, Castaldo G. Corrigendum: Age-Related Differences in the Expression of Most Relevant Mediators of SARS-CoV-2 Infection in Human Respiratory and Gastrointestinal Tract. *Front Pediatr*. 2021 Nov 10;9:790285. doi: 10.3389/fped.2021.790285. PMID: 34858910; PMCID: PMC8631725.

Comegna M, Terlizzi V, Salvatore D, Colangelo C, Di Lullo AM, **Zollo I**, Taccetti G, Castaldo G, Amato F. Elexacaftor-Tezacaftor-Ivacaftor Therapy for Cystic Fibrosis Patients with The F508del/Unknown Genotype. *Antibiotics* (Basel). 2021 Jul 7;10(7):828. doi: 10.3390/antibiotics10070828. PMID: 34356748; PMCID: PMC8300667.

Lo Cicero S, Castelli G, Blaconà G, Bruno S, Sette G, Pigliucci R, Villella VR, Esposito S, **Zollo I**, De Maria R, Biffoni M, Cimino G, Amato F, Lucarelli M, Eramo A. L1077P CFTR pathogenic variant function rescue by Trikafta in cystic fibrosis patient-derived ALI-cultures and organoids: in-vitro guided personalized therapy of non-F508del patients. S*ubmitted to Respiratory Research.*

Kleinfelder K, Lotti V, Eramo A, Amato F, Farinazzo A, Dell'Orco D, Preato S, Conti J, Rodella L, Tomba F, Cerofolini A, Baldisseri E, Bertini M, Volpi S, Lo Cicero S, Castelli G, Villella VR, Esposito S, **Zollo I**, Laudanna C, Lucarelli M, Melotti P, Sorio C. In silico analysis and theratyping of an ultra-rare CFTR genotype (W57G/A234D) in primary human rectal and nasal epithe-lial cells. *Submitted to iScience.*

Cortese P, Amato F, D'Avino A, De Franchis R, Esposito S, **Zollo I**, Di Domenico M, Solito E, Zarrilli F, Gentile L, Cernera G, Castaldo G. Humoral and cellular response to Sars-CoV-2 vaccine in a cohort of Family Pediatricians from Southern Italy. *Submitted to International Journal of Molecular Sciences.*

8. REFERENCES

Aggarwal P, Kehoe S. Serum tumour markers in gynaecological cancers. *Maturitas*. 2010;67(1):46-53.

Alper Seyhan. Factors Affecting the Diagnostic Accuracy of Endometrial Pipelle® Biopsy. *Bagcilar Med Bull* 2021;6(4):370-375.

Ameer MA, Fagan SE, Sosa-Stanley JN, Peterson DC. Anatomy, Abdomen and Pelvis, Uterus. 2022 Feb 23. In: StatPearls [Internet]. Treasure Island (FL): StatPearls Publishing; 2022.

Angioli R, Plotti F, Capriglione S, Montera R, Damiani P, Ricciardi R, Aloisi A, Luvero D, Cafà EV, Dugo N, Angelucci M, Benedetti-Panici P. The role of novel biomarker HE4 in endometrial cancer: a case control prospective study. *Tumour Biol*. 2013;34(1):571-6.

Antill Y, Kok PS, Robledo K, Yip S, Cummins M, Smith D, Spurdle A, Barnes E, Lee YC, Friedlander M, Baron-Hay S, Shannon C, Coward J, Beale P, Goss G, Meniawy T, Lombard J, Andrews J, Stockler MR, Mileshkin L; Australia New Zealand Gynaecological Oncology Group (ANZGOG). Clinical activity of durvalumab for patients with advanced mismatch repair-deficient and repair-proficient endometrial cancer. A nonrandomized phase 2 clinical trial. *J Immunother Cancer*. 2021;9(6):e002255.

Antonsen SL, Høgdall E, Christensen IJ, Lydolph M, Tabor A, Loft Jakobsen A, Fagö-Olsen CL, Andersen ES, Jochumsen K, Høgdall C. HE4 and CA125 levels in the preoperative assessment of endometrial cancer patients: a prospective multicenter study (ENDOMET). *Acta Obstet Gynecol Scand*. 2013;92(11):1313-22.

Aslan F, Güney G, Avcıkurt AS, Taşkın MI, Akgün GA. Relationship Between CIP2A and Endometrium Cancer. *J Coll Physicians Surg Pak*. 2020;30(4):373-378.

Badshah MA, Koh NY, Zia AW, Abbas N, Zahra Z, Saleem MW. Recent Developments in Plasmonic Nanostructures for Metal Enhanced Fluorescence-Based Biosensing. *Nanomaterials (Basel)*. 2020;10(9):1749.

Balzar M, Winter MJ, de Boer CJ, Litvinov SV. The biology of the 17-1A antigen (Ep-CAM). *J Mol Med (Berl)*. 1999;77(10):699-712.

Barisciano G, Colangelo T, Rosato V, Muccillo L, Taddei ML, Ippolito L, Chiarugi P, Galgani M, Bruzzaniti S, Matarese G, Fassan M, Agostini M, Bergamo F, Pucciarelli S, Carbone A, Mazzoccoli G, Colantuoni V, Bianchi F,

Sabatino L. miR-27a is a master regulator of metabolic reprogramming and chemoresistance in colorectal cancer. *Br J Cancer*. 2020;122(9):1354-1366.

Barra F, Evangelisti G, Ferro Desideri L, Di Domenico S, Ferraioli D, Vellone VG, De Cian F, Ferrero S. Investigational PI3K/AKT/mTOR inhibitors in development for endometrial cancer. *Expert Opin Investig Drugs*. 2019;28(2):131-142.

Bartel DP. Metazoan MicroRNAs. *Cell*. 2018;173(1):20-51.

Behrouzi R, Barr CE, Crosbie EJ. HE4 as a Biomarker for Endometrial Cancer. *Cancers (Basel)*. 2021;13(19):4764.

Benati M, Montagnana M, Danese E, Paviati E, Giudici S, Ruzzenente O, Franchi M, Lippi G. The clinical significance of DJ-1 and HE4 in patients with endometrial cancer. *J Clin Lab Anal*. 2018;32(1):e22223.

Bingle L, Singleton V, Bingle CD. The putative ovarian tumour marker gene HE4 (WFDC2), is expressed in normal tissues and undergoes complex alternative splicing to yield multiple protein isoforms. *Oncogene*. 2002;21(17):2768-73.

Bokhman JV. Two pathogenetic types of endometrial carcinoma. *Gynecol Oncol*. 1983; 15: 10–17

Bouchard D, Morisset D, Bourbonnais Y, Tremblay GM. Proteins with whey-acidic-protein motifs and cancer. *Lancet Oncol*. 2006;7(2):167-74.

Cancer Genome Atlas Research Network, Kandoth C, Schultz N, Cherniack AD, Akbani R, Liu Y, Shen H, Robertson AG, Pashtan I, Shen R, Benz CC, Yau C, Laird PW, Ding L, Zhang W, Mills GB, Kucherlapati R, Mardis ER, Levine DA. Integrated genomic characterization of endometrial carcinoma. *Nature*. 2013;500(7461):242.

Chaudhry SR, Chaudhry K. Anatomy, Abdomen and Pelvis, Uterus Round Ligament. 2021 Jul 26. In: StatPearls [Internet]. Treasure Island (FL): StatPearls Publishing; 2022.

Chaves-Pérez A, Mack B, Maetzel D, Kremling H, Eggert C, Harréus U, Gires O. EpCAM regulates cell cycle progression via control of cyclin D1 expression. *Oncogene*. 2013;32(5):641-50.

Cheng D, Sun Y, He H. Diagnostic role of circulating YKL-40 in endometrial carcinoma patients: a meta-analysis of seven related studies. *Med Oncol*. 2014;31(12):326.

Choi YA, Koo JS, Park JS, Park MY, Jeong AL, Oh KS, Yang Y. Estradiol enhances CIP2A expression by the activation of p70 S6 kinase. *Endocr Relat Cancer*. 2014;21(2):189-202.

Choi YA, Park JS, Park MY, Oh KS, Lee MS, Lim JS, Kim KI, Kim KY, Kwon J, Yoon DY, Moon EY, Yang Y. Increase in CIP2A expression is associated with doxorubicin resistance. *FEBS Lett*. 2011;585(5):755-60.

Clark TJ, Voit D, Gupta JK, Hyde C, Song F, Khan KS. Accuracy of hysteroscopy in the diagnosis of endometrial cancer and hyperplasia: a systematic quantitative review. *JAMA*. 2002;288(13):1610-21.

Clarke MA, Long BJ, Del Mar Morillo A, Arbyn M, Bakkum-Gamez JN, Wentzensen N. Association of Endometrial Cancer Risk With Postmenopausal Bleeding in Women: A Systematic Review and Meta-analysis. JAMA Intern Med. 2018;178(9):1210-1222.

Côme C, Laine A, Chanrion M, Edgren H, Mattila E, Liu X, Jonkers J, Ivaska J, Isola J, Darbon JM, Kallioniemi O, Thézenas S, Westermarck J. CIP2A is associated with human breast cancer aggressivity. *Clin Cancer Res*. 2009;15(16):5092-100.

Cote ML, Ruterbusch JJ, Olson SH, Lu K, Ali-Fehmi R. The Growing Burden of Endometrial Cancer: A Major Racial Disparity Affecting Black Women. *Cancer Epidemiol Biomarkers Prev*. 2015;24(9):1407-15.

Coutinho C, Somoza Á. MicroRNA sensors based on gold nanoparticles. Anal Bioanal Chem. 2019;411(9):1807-1824.

Creasman W. Revised FIGO staging for carcinoma of the endometrium. *Int J Gynaecol Obstet*. 2009;105(2):109.

Cuesta-Guardiola T, Carretero AQ, Martinez-Martinez J, Cuñarro-López Y, Pereira-Sánchez A, Fernández-Corona A, de Leon-Luis JA. Identification and characterization of endometrial carcinoma with tumor markers HE4 and CA125 in serum and endometrial tissue samples. *J Turk Ger Gynecol Assoc*. 2021;22(3):161-167.

Cui Q, He F, Li L, Möhwald H. Controllable metal-enhanced fluorescence in organized films and colloidal system. *Adv Colloid Interface Sci*. 2014;207:164-77.

Davidson KG, Dubinsky TJ. Ultrasonographic evaluation of the endometrium in postmenopausal vaginal bleeding. *Radiol Clin North Am*. 2003;41(4):769-80.

Della Ventura B, Banchelli M, Funari R, Illiano A, De Angelis M, Taroni P, Amoresano A, Matteini P, Velotta R. Biosensor surface functionalization by a simple photochemical immobilization of antibodies: experimental characterization by mass spectrometry and surface enhanced Raman spectroscopy. *Analyst*. 2019a;144(23):6871-6880.

Della Ventura B, Gelzo M, Battista E, Alabastri A, Schirato A, Castaldo G, Corso G, Gentile F, Velotta R. Biosensor for Point-of-Care Analysis of Immunoglobulins in Urine by Metal Enhanced Fluorescence from Gold Nanoparticles. *ACS Appl Mater Interfaces*. 2019b;11(4):3753-3762.

Dochez V, Caillon H, Vaucel E, Dimet J, Winer N, Ducarme G. Biomarkers and algorithms for diagnosis of ovarian cancer: CA125, HE4, RMI and ROMA, a review. *J Ovarian Res*. 2019;12(1):28.

Doll A, Abal M, Rigau M, Monge M, Gonzalez M, Demajo S, Colás E, Llauradó M, Alazzouzi H, Planagumá J, Lohmann MA, Garcia J, Castellvi S, Ramon y Cajal J, Gil-Moreno A, Xercavins J, Alameda F, Reventós J. Novel molecular profiles of endometrial cancer-new light through old windows. *J Steroid Biochem Mol Biol.* 2008;108(3-5):221-9.

Espiau Romera A, Cuesta Guardiola T, Benito Vielba M, De Bonrostro Torralba C, Coronado Martín PJ, Baquedano Mainar L. HE4 tumor marker as a predictive factor for lymphatic metastasis in endometrial cancer. *Int J Gynaecol Obstet*. 2020;149(3):265-268.

Esposito MT, So CW. DNA damage accumulation and repair defects in acute myeloid leukemia: implications for pathogenesis, disease progression, and chemotherapy resistance. *Chromosoma*. 2014;123(6):545-61.

Fan J, Ren H, Jia N, Fei E, Zhou T, Jiang P, Wu M, Wang G. DJ-1 decreases Bax expression through repressing p53 transcriptional activity. *J Biol Chem*. 2008;283(7):4022-30.

Fang Y, Li Z, Wang X, Zhang S. CIP2A is overexpressed in human ovarian cancer and regulates cell proliferation and apoptosis. *Tumour Biol*. 2012;33(6):2299-306.

Francescone RA, Scully S, Faibish M, Taylor SL, Oh D, Moral L, Yan W, Bentley B, Shao R. Role of YKL-40 in the angiogenesis, radioresistance, and progression of glioblastoma. *J Biol Chem*. 2011;286(17):15332-43.

Galgano MT, Hampton GM, Frierson HF Jr. Comprehensive analysis of HE4 expression in normal and malignant human tissues. *Mod Pathol*. 2006;19(6):847-53.

Gasner A, Aatsha PA. Physiology, Uterus. 2022 May 19. In: StatPearls [Internet]. Treasure Island (FL): StatPearls Publishing; 2022 Jan–. PMID: 32491507

Geldenhuys L, Murray ML. Sensitivity and specificity of the Pap smear for glandular lesions of the cervix and endometrium. *Acta Cytol*. 2007;51(1):47-50.

Ghazala RA, El-Attar EA, Abouzeid ZS. Circulating miRNA 27a and miRNA150-5p; a noninvasive approach to endometrial carcinoma. *Mol Biol Rep*. 2021;48(5):4351-4360.

Gu B, Shang X, Yan M, Li X, Wang W, Wang Q, Zhang C. Variations in incidence and mortality rates of endometrial cancer at the global, regional, and national levels, 1990-2019. *Gynecol Oncol*. 2021;161(2):573-580.

Gupta JK, Chien PF, Voit D, Clark TJ, Khan KS. Ultrasonographic endometrial thickness for diagnosing endometrial pathology in women with postmenopausal bleeding: a meta-analysis. *Acta Obstet Gynecol Scand*. 2002;81(9):799-816.

Hakala BE, White C, Recklies AD. Human cartilage gp-39, a major secretory product of articular chondrocytes and synovial cells, is a mammalian member of a chitinase protein family. *J Biol Chem*. 1993;268(34):25803-10.

Hao L, Wang J. miR-27a acts as an oncogene to regulate endometrial cancer progression by targeting USP46. *Int J Clin Exp Pathol*. 2021;14(6):720-725.

Hashmi AA, Iftikhar SN, Ali J, Shaheen F, Afroze F, Imran A. Morphological Spectrum and Pathological Parameters of Type 2 Endometrial Carcinoma: A Comparison With Type 1 Endometrial Cancers. *Cureus*. 2020;12(10):e11025.

He TC, Sparks AB, Rago C, Hermeking H, Zawel L, da Costa LT, Morin PJ, Vogelstein B, Kinzler KW. Identification of c-MYC as a target of the APC pathway. *Science*. 1998;281(5382):1509-12.

He W, Qin M, Cai Y, Gao X, Cao S, Wang Z, Chen H, Xu R. Downregulation of HOXC6 by miR-27a ameliorates gefitinib resistance in non-small cell lung cancer. *Am J Cancer Res*. 2021;11(9):4329-4346.

Herlyn M, Steplewski Z, Herlyn D, Koprowski H. Colorectal carcinoma-specific antigen: detection by means of monoclonal antibodies. *Proc Natl Acad Sci USA*. 1979;76(3):1438-42.

Hwang WY, Suh DH, Kim K, No JH, Kim YB. Aspiration biopsy versus dilatation and curettage for endometrial hyperplasia prior to hysterectomy. *Diagn Pathol*. 2021;16(1):7.

Janssens V, Goris J. Protein phosphatase 2A: a highly regulated family of serine/threonine phosphatases implicated in cell growth and signalling. *Biochem J*. 2001;353(Pt 3):417-39.

Jayanthi VSPKSA, Das AB, Saxena U. Recent advances in biosensor development for the detection of cancer biomarkers. *Biosens Bioelectron*. 2017;91:15-23.

Jia W, Wu Y, Zhang Q, Gao G, Zhang C, Xiang Y. Identification of four serum microRNAs from a genome-wide serum microRNA expression profile as potential non-invasive biomarkers for endometrioid endometrial cancer. *Oncol Lett*. 2013;6(1):261-267.

Jiang P, Du W, Wu M. Regulation of the pentose phosphate pathway in cancer. Protein Cell. 2014;5(8):592-602.

Jiang SW, Chen H, Dowdy S, Fu A, Attewell J, Kalogera E, Drapkin R, Podratz K, Broaddus R, Li J. HE4 transcription- and splice variants-specific expression in endometrial cancer and correlation with patient survival. *Int J Mol Sci*. 2013;14(11):22655-77.

Johansen JS, Jensen BV, Roslind A, Nielsen D, Price PA. Serum YKL-40, a new prognostic biomarker in cancer patients? *Cancer Epidemiol Biomarkers Prev*. 2006;15(2):194-202.

Johansen JS, Williamson MK, Rice JS, Price PA. Identification of proteins secreted by human osteoblastic cells in culture. *J Bone Miner Res*. 1992;7(5):501-12.

Junttila MR, Puustinen P, Niemelä M, Ahola R, Arnold H, Böttzauw T, Ala-aho R, Nielsen C, Ivaska J, Taya Y, Lu SL, Lin S, Chan EK, Wang XJ, Grènman R, Kast J, Kallunki T, Sears R, Kähäri VM, Westermarck J. CIP2A inhibits PP2A in human malignancies. *Cell*. 2007;130(1):51-62.

Kaaks R, Lukanova A, Kurzer MS. Obesity, endogenous hormones, and endometrial cancer risk: a synthetic review. *Cancer Epidemiol Biomarkers Prev*. 2002;11(12):1531-43.

Kauko O, Westermarck J. Non-genomic mechanisms of protein phosphatase 2A (PP2A) regulation in cancer. *Int J Biochem Cell Biol*. 2018;96:157-164.

Kemik P, Saatli B, Yıldırım N, Kemik VD, Deveci B, Terek MC, Koçtürk S, Koyuncuoğlu M, Saygılı U. Diagnostic and prognostic values of preoperative serum levels of YKL-40, HE-4 and DKK-3 in endometrial cancer. *Gynecol Oncol*. 2016;140(1):64-9.

Kim RH, Peters M, Jang Y, Shi W, Pintilie M, Fletcher GC, DeLuca C, Liepa J, Zhou L, Snow B, Binari RC, Manoukian AS, Bray MR, Liu FF, Tsao MS, Mak TW. DJ-1, a novel regulator of the tumor suppressor PTEN. *Cancer Cell*. 2005;7(3):263-73.

Kirchhoff C, Habben I, Ivell R, Krull N. A major human epididymis-specific cDNA encodes a protein with sequence homology to extracellular proteinase inhibitors. *Biol Reprod*. 1991;45(2):350-7.

Kuhn E, Bahadirli-Talbott A, Shih IeM. Frequent CCNE1 amplification in endometrial intraepithelial carcinoma and uterine serous carcinoma. *Mod Pathol*. 2014;27(7):1014-9.

Kuo LJ, Yang LX. Gamma-H2AX - a novel biomarker for DNA double-strand breaks. *In Vivo*. 2008;22(3):305-9.

Kurnit KC, Kim GN, Fellman BM, Urbauer DL, Mills GB, Zhang W, Broaddus RR. CTNNB1 (beta-catenin) mutation identifies low grade, early stage endometrial cancer patients at increased risk of recurrence. *Mod Pathol*. 2017;30(7):1032-1041.

Laine A, Sihto H, Come C, Rosenfeldt MT, Zwolinska A, Niemelä M, Khanna A, Chan EK, Kähäri VM, Kellokumpu-Lehtinen PL, Sansom OJ, Evan GI, Junttila MR, Ryan KM, Marine JC, Joensuu H, Westermarck J. Senescence sensitivity of breast cancer cells is defined by positive feedback loop between CIP2A and E2F1. *Cancer Discov*. 2013;3(2):182-97.

Lambrecht C, Haesen D, Sents W, Ivanova E, Janssens V. Structure, regulation, and pharmacological modulation of PP2A phosphatases. *Methods Mol Biol*. 2013;1053:283-305.

Lan T, Mu C, Wang Z, Wang Y, Li Y, Mai Y, Li S, Xu H, Gu B, Luo L, Ma P. Diagnostic and Prognostic Values of Serum EpCAM, TGM2, and HE4 Levels in Endometrial Cancer. *Front Oncol*. 2020;10:1697.

Laurent G, Jaffrézou JP. Signaling pathways activated by daunorubicin. *Blood*. 2001;98(4):913-24.

Lee YS, Dutta A. MicroRNAs in cancer. *Annu Rev Pathol*. 2009;4:199-227.

León-Castillo A, Gilvazquez E, Nout R, Smit VT, McAlpine JN, McConechy M, Kommoss S, Brucker SY, Carlson JW, Epstein E, Rau TT, Soslow RA, Ganesan R, Matias-Guiu X, Oliva E, Harrison BT, Church DN, Gilks CB, Bosse T. Clinicopathological and molecular characterisation of 'multiple-classifier' endometrial carcinomas. *J Pathol*. 2020;250(3):312-322.

Lewin SN, Herzog TJ, Barrena Medel NI, Deutsch I, Burke WM, Sun X, Wright JD. Comparative performance of the 2009 international Federation of gynecology and obstetrics' staging system for uterine corpus cancer. *Obstet Gynecol*. 2010;116(5):1141-9.

Li J, Chen H, Mariani A, Chen D, Klatt E, Podratz K, Drapkin R, Broaddus R, Dowdy S, Jiang SW. HE4 (WFDC2) Promotes Tumor Growth in Endometrial Cancer Cell Lines. *Int J Mol Sci*. 2013;14(3):6026-43.

Li W, Zhang H, Yang L, Wang Y. Cancerous inhibitor of protein phosphatase 2A regulates cisplatin resistance in ovarian cancer. *Oncol Lett*. 2019;17(1):1211-1216

Li X, Stevens PD, Yang H, Gulhati P, Wang W, Evers BM, Gao T. The deubiquitination enzyme USP46 functions as a tumor suppressor by controlling PHLPP-dependent attenuation of Akt signaling in colon cancer. *Oncogene*. 2013;32(4):471-8.

Li Y, Tian Z, Tan Y, Lian G, Chen S, Chen S, Li J, Li X, Huang K, Chen Y. Bmi-1-induced miR-27a and miR-155 promote tumor metastasis and chemoresistance by targeting RKIP in gastric cancer. *Mol Cancer*. 2020;19(1):109.

Liaw JW, Tsai HY, Huang CH. Size-Dependent Surface Enhanced Fluorescence of Gold Nanorod: Enhancement or Quenching. *Plasmonics*. 2012; 7:543–553

Liu CY, Hsieh FS, Chu PY, Tsai WC, Huang CT, Yu YB, Huang TT, Ko PS, Hung MH, Wang WL, Shiau CW, Chen KF. Carfilzomib induces leukaemia cell apoptosis via inhibiting ELK1/KIAA1524 (Elk-1/CIP2A) and activating PP2A not related to proteasome inhibition. *Br J Haematol*. 2017a;177(5):726-740.

Liu CY, Huang TT, Huang CT, Hu MH, Wang DS, Wang WL, Tsai WC, Lee CH, Lau KY, Yang HP, Chen MH, Shiau CW, Tseng LM, Chen KF. EGFR-independent Elk1/CIP2A signalling mediates apoptotic effect of an erlotinib derivative TD52 in triple-negative breast cancer cells. *Eur J Cancer*. 2017b;72:112-123.

Liu J, Wang M, Zhang X, Wang Q, Qi M, Hu J, Zhou Z, Zhang C, Zhang W, Zhao W, Wang X. CIP2A is associated with multidrug resistance in cervical adenocarcinoma by a P-glycoprotein pathway. *Tumour Biol*. 2016;37(2):2673-82.

Liu Y, Patel L, Mills GB, Lu KH, Sood AK, Ding L, Kucherlapati R, Mardis ER, Levine DA, Shmulevich I, Broaddus RR, Zhang W. Clinical significance

of CTNNB1 mutation and Wnt pathway activation in endometrioid endometrial carcinoma. *J Natl Cancer Inst*. 2014;106(9):dju245.

Lucas CM, Harris RJ, Giannoudis A, Copland M, Slupsky JR, Clark RE. Cancerous inhibitor of PP2A (CIP2A) at diagnosis of chronic myeloid leukemia is a critical determinant of disease progression. *Blood*. 2011;117(24):6660-8.

Maetzel D, Denzel S, Mack B, Canis M, Went P, Benk M, Kieu C, Papior P, Baeuerle PA, Munz M, Gires O. Nuclear signalling by tumour-associated antigen EpCAM. *Nat Cell Biol*. 2009;11(2):162-71.

Marabelle A, Le DT, Ascierto PA, Di Giacomo AM, De Jesus-Acosta A, Delord JP, Geva R, Gottfried M, Penel N, Hansen AR, Piha-Paul SA, Doi T, Gao B, Chung HC, Lopez-Martin J, Bang YJ, Frommer RS, Shah M, Ghori R, Joe AK, Pruitt SK, Diaz LA Jr. Efficacy of Pembrolizumab in Patients With Noncolorectal High Microsatellite Instability/Mismatch Repair-Deficient Cancer: Results From the Phase II KEYNOTE-158 Study. *J Clin Oncol*. 2020;38(1):1-10.

McConechy MK, Anglesio MS, Kalloger SE, Yang W, Senz J, Chow C, Heravi-Moussavi A, Morin GB, Mes-Masson AM; Australian Ovarian Cancer Study Group, Carey MS, McAlpine JN, Kwon JS, Prentice LM, Boyd N, Shah SP, Gilks CB, Huntsman DG. Subtype-specific mutation of PPP2R1A in endometrial and ovarian carcinomas. *J Pathol*. 2011;223(5):567-73.

Miller DM, Thomas SD, Islam A, Muench D, Sedoris K. c-Myc and cancer metabolism. *Clin Cancer Res*. 2012;18(20):5546-53.

Morelli M, Scumaci D, Di Cello A, Venturella R, Donato G, Faniello MC, Quaresima B, Cuda G, Zullo F, Costanzo F. DJ-1 in endometrial cancer: a possible biomarker to improve differential diagnosis between subtypes. *Int J Gynecol Cancer*. 2014;24(4):649-58.

Münz M, Kieu C, Mack B, Schmitt B, Zeidler R, Gires O. The carcinoma-associated antigen EpCAM upregulates c-myc and induces cell proliferation. *Oncogene*. 2004;23(34):5748-58.

Nagakubo D, Taira T, Kitaura H, Ikeda M, Tamai K, Iguchi-Ariga SM, Ariga H. DJ-1, a novel oncogene which transforms mouse NIH3T3 cells in cooperation with ras. *Biochem Biophys Res Commun*. 1997;231(2):509-13.

O'Doherty U, Swiggard WJ, Malim MH. Human immunodeficiency virus type 1 spinoculation enhances infection through virus binding. *J Virol*. 2000;74(21):10074-80.

Oh SE, Mouradian MM. Regulation of Signal Transduction by DJ-1. *Adv Exp Med Biol*. 2017;1037:97-131.

Pallai R, Bhaskar A, Sodi V, Rice LM. Ets1 and Elk1 transcription factors regulate cancerous inhibitor of protein phosphatase 2A expression in cervical and endometrial carcinoma cells. *Transcription*. 2012;3(6):323-35.

Panyavaranant P, Manchana T. Preoperative markers for the prediction of high-risk features in endometrial cancer. *World J Clin Oncol*. 2020;11(6):378-388.

Park AB, Darcy KM, Tian C, Casablanca Y, Schinkel JK, Enewold L, McGlynn KA, Shriver CD, Zhu K. Racial disparities in survival among women with endometrial cancer in an equal access system. *Gynecol Oncol.* 2021;163(1):125-129.

Parsanejad M, Zhang Y, Qu D, Irrcher I, Rousseaux MW, Aleyasin H, Kamkar F, Callaghan S, Slack RS, Mak TW, Lee S, Figeys D, Park DS. Regulation of the VHL/HIF-1 pathway by DJ-1. *J Neurosci*. 2014;34(23):8043-50.

Patra KC, Hay N. The pentose phosphate pathway and cancer. *Trends Biochem Sci*. 2014;39(8):347-54.

Patriarca C, Macchi RM, Marschner AK, Mellstedt H. Epithelial cell adhesion molecule expression (CD326) in cancer: a short review. *Cancer Treat Rev*. 2012;38(1):68-75.

Peng B, Lei N, Chai Y, Chan EK, Zhang JY. CIP2A regulates cancer metabolism and CREB phosphorylation in non-small cell lung cancer. *Mol Biosyst*. 2015;11(1):105-14.

Peungjesada S, Bhosale PR, Balachandran A, Iyer RB. Magnetic resonance imaging of endometrial carcinoma. *J Comput Assist Tomogr*. 2009;33(4):601-8.

Pfaffl MW. A new mathematical model for relative quantification in real-time RT-PCR. Nucleic Acids Res. 2001;29(9):e45.

Ravegnini G, Gorini F, De Crescenzo E, De Leo A, De Biase D, Di Stanislao M, Hrelia P, Angelini S, De Iaco P, Perrone AM. Can miRNAs be useful biomarkers in improving prognostic stratification in endometrial cancer patients? An update review. *Int J Cancer*. 2022;150(7):1077-1090.

Remmerie M, Janssens V. PP2A: A Promising Biomarker and Therapeutic Target in Endometrial Cancer. *Front Oncol.* 2019;9:462.

Ren J, Li W, Yan L, Jiao W, Tian S, Li D, Tang Y, Gu G, Liu H, Xu Z. Expression of CIP2A in renal cell carcinomas correlates with tumour invasion, metastasis and patients' survival. *Br J Cancer*. 2011;105(12):1905-11.

Rusling JF, Kumar CV, Gutkind JS, Patel V. Measurement of biomarker proteins for point-of-care early detection and monitoring of cancer. *Analyst*. 2010;135(10):2496-511.

Sakamoto S, Putalun W, Vimolmangkang S, Phoolcharoen W, Shoyama Y, Tanaka H, Morimoto S. Enzyme-linked immunosorbent assay for the quantitative/qualitative analysis of plant secondary metabolites. *J Nat Med*. 2018;72(1):32-42.

Sawicki LM, Kirchner J, Grueneisen J, Ruhlmann V, Aktas B, Schaarschmidt BM, Forsting M, Herrmann K, Antoch G, Umutlu L. Comparison of ^{18}F-FDG PET/MRI and MRI alone for whole-body staging and potential impact on therapeutic management of women with suspected recurrent pelvic cancer: a follow-up study. *Eur J Nucl Med Mol Imaging*. 2018;45(4):622-629.

Seshacharyulu P, Pandey P, Datta K, Batra SK. Phosphatase: PP2A structural importance, regulation and its aberrant expression in cancer. *Cancer Lett*. 2013;335(1):9-18.

Shao R, Hamel K, Petersen L, Cao QJ, Arenas RB, Bigelow C, Bentley B, Yan W. YKL-40, a secreted glycoprotein, promotes tumor angiogenesis. *Oncogene*. 2009;28(50):4456-68.

Sharma A, Singh K, Almasan A. Histone H2AX phosphorylation: a marker for DNA damage. *Methods Mol Biol*. 2012;920:613-26

Shu K, Xiao Z, Long S, Yan J, Yu X, Zhu Q, Mei T. Expression of DJ-1 in endometrial cancer: close correlation with clinicopathological features and apoptosis. *Int J Gynecol Cancer*. 2013;23(6):1029-35.

Siegel RL, Miller KD, Fuchs HE, Jemal A. Cancer Statistics, 2021. *CA Cancer J Clin*. 2021; 71(4):359.

Slomovitz BM, Coleman RL. The PI3K/AKT/mTOR pathway as a therapeutic target in endometrial cancer. *Clin Cancer Res*. 2012;18(21):5856-64.

Smith-Bindman R, Kerlikowske K, Feldstein VA, Subak L, Scheidler J, Segal M, Brand R, Grady D. Endovaginal ultrasound to exclude endometrial cancer and other endometrial abnormalities. JAMA. 1998;280(17):1510-7.

Smotkin D, Nevadunsky NS, Harris K, Einstein MH, Yu Y, Goldberg GL. Histopathologic differences account for racial disparity in uterine cancer survival. Gynecol Oncol. 2012;127(3):616-9.

Sohel MMH. Circulating microRNAs as biomarkers in cancer diagnosis. *Life Sci*. 2020;248:117473.

Stelloo E, Nout RA, Osse EM, Jürgenliemk-Schulz IJ, Jobsen JJ, Lutgens LC, van der Steen-Banasik EM, Nijman HW, Putter H, Bosse T, Creutzberg CL, Smit VT. Improved Risk Assessment by Integrating Molecular and Clinicopathological Factors in Early-stage Endometrial Cancer-Combined Analysis of the PORTEC Cohorts. *Clin Cancer Res*. 2016;22(16):4215-24.

Stiekema A, Lok C, Korse CM, van Driel WJ, van der Noort V, Kenter GG, Van de Vijver KK. Serum HE4 is correlated to prognostic factors and survival in patients with endometrial cancer. *Virchows Arch*. 2017;470(6):655-664.

Strobbia P, Languirand E, Cullum BM. Recent Advances in Plasmonic Nanostructures for Sensing: A Review. *Opt. Eng*. 2015;54(10),100902

Svanvik T, Marcickiewicz J, Sundfeldt K, Holmberg E, Strömberg U. Sociodemographic disparities in stage-specific incidences of endometrial cancer: a registry-based study in West Sweden, 1995-2016. *Acta Oncol*. 2019;58(6):845-851.

Talhouk A, McConechy MK, Leung S, Yang W, Lum A, Senz J, Boyd N, Pike J, Anglesio M, Kwon JS, Karnezis AN, Huntsman DG, Gilks CB, McAlpine JN. Confirmation of ProMisE: A simple, genomics-based clinical classifier for endometrial cancer. *Cancer*. 2017;123(5):802-813.

Tarney CM, Tian C, Wang G, Dubil EA, Bateman NW, Chan JK, Elshaikh MA, Cote ML, Schildkraut JM, Shriver CD, Conrads TP, Hamilton CA, Maxwell GL, Darcy KM. Impact of age at diagnosis on racial disparities in endometrial cancer patients. *Gynecol Oncol*. 2018;149(1):12-21.

Timmermans A, Opmeer BC, Khan KS, Bachmann LM, Epstein E, Clark TJ, Gupta JK, Bakour SH, van den Bosch T, van Doorn HC, Cameron ST, Giusa MG, Dessole S, Dijkhuizen FPHLJ, Ter Riet G, Mol BWJ. Endometrial thickness measurement for detecting endometrial cancer in women with postmenopausal bleeding: a systematic review and meta-analysis. *Obstet Gynecol*. 2010;116(1):160-167.

Torres A, Pac-Sosińska M, Wiktor K, Paszkowski T, Maciejewski R, Torres K. CD44, TGM2 and EpCAM as novel plasma markers in endometrial cancer diagnosis. *BMC Cancer*. 2019;19(1):401.

Troisi J, Raffone A, Travaglino A, Belli G, Belli C, Anand S, Giugliano L, Cavallo P, Scala G, Symes S, Richards S, Adair D, Fasano A, Bottigliero V, Guida M. Development and Validation of a Serum Metabolomic Signature for

Endometrial Cancer Screening in Postmenopausal Women. *JAMA Netw Open*. 2020;3(9):e2018327.

Troisi J, Sarno L, Landolfi A, Scala G, Martinelli P, Venturella R, Di Cello A, Zullo F, Guida M. Metabolomic Signature of Endometrial Cancer. *J Proteome Res*. 2018;17(2):804-812.

Tsukamoto O, Miura K, Mishima H, Abe S, Kaneuchi M, Higashijima A, Miura S, Kinoshita A, Yoshiura K, Masuzaki H. Identification of endometrioid endometrial carcinoma-associated microRNAs in tissue and plasma. *Gynecol Oncol*. 2014;132(3):715-21.

van den Heerik ASVM, Horeweg N, de Boer SM, Bosse T, Creutzberg CL. Adjuvant therapy for endometrial cancer in the era of molecular classification: radiotherapy, chemoradiation and novel targets for therapy. *Int J Gynecol Cancer*. 2021;31(4):594-604.

van Gool IC, Eggink FA, Freeman-Mills L, Stelloo E, Marchi E, de Bruyn M, Palles C, Nout RA, de Kroon CD, Osse EM, Klenerman P, Creutzberg CL, Tomlinson IP, Smit VT, Nijman HW, Bosse T, Church DN. POLE Proofreading Mutations Elicit an Antitumor Immune Response in Endometrial Cancer. *Clin Cancer Res*. 2015;21(14):3347-3355.

Wang J, Li W, Li L, Yu X, Jia J, Chen C. CIP2A is over-expressed in acute myeloid leukaemia and associated with HL60 cells proliferation and differentiation. *Int J Lab Hematol*. 2011;33(3):290-8.

Wang L, Chen YJ, Xu K, Xu H, Shen XZ, Tu RQ. Circulating microRNAs as a fingerprint for endometrial endometrioid adenocarcinoma. *PLoS One*. 2014;9(10):e110767.

Wang L, Gu F, Ma N, Zhang L, Bian JM, Cao HY. CIP2A expression is associated with altered expression of epithelial-mesenchymal transition markers and predictive of poor prognosis in pancreatic ductal adenocarcinoma. *Tumour Biol*. 2013;34(4):2309-13.

Wang Y, Li L, Douville C, Cohen JD, Yen TT, Kinde I, Sundfelt K, Kjær SK, Hruban RH, Shih IM, Wang TL, Kurman RJ, Springer S, Ptak J, Popoli M, Schaefer J, Silliman N, Dobbyn L, Tanner EJ, Angarita A, Lycke M, Jochumsen K, Afsari B, Danilova L, Levine DA, Jardon K, Zeng X, Arseneau J, Fu L, Diaz LA Jr, Karchin R, Tomasetti C, Kinzler KW, Vogelstein B, Fader AN, Gilbert L, Papadopoulos N. Evaluation of liquid from the Papanicolaou test and other liquid biopsies for the detection of endometrial and ovarian cancers. *Sci Transl Med*. 2018;10(433):eaap8793.

Wright JD, Fiorelli J, Schiff PB, Burke WM, Kansler AL, Cohen CJ, Herzog TJ. Racial disparities for uterine corpus tumors: changes in clinical characteristics and treatment over time. *Cancer*. 2009;115(6):1276-85.

Xu Y, Sengupta T, Kukreja L, Minella AC. MicroRNA-223 regulates cyclin E activity by modulating expression of F-box and WD-40 domain protein 7. *J Biol Chem*. 2010;285(45):34439-46.

Yamashita T, Budhu A, Forgues M, Wang XW. Activation of hepatic stem cell marker EpCAM by Wnt-beta-catenin signaling in hepatocellular carcinoma. *Cancer Res*. 2007;67(22):10831-9.

Yen TT, Wang TL, Fader AN, Shih IM, Gaillard S. Molecular Classification and Emerging Targeted Therapy in Endometrial Cancer. *Int J Gynecol Pathol*. 2020;39(1):26-35.

Yu H, Peng Y, Yang Y, Li ZY. Plasmon-enhanced light–matter interactions and applications. *npj Comput Mater*. **5**, 45 (2019).

Yu N, Zhang T, Zhao D, Cao Z, Du J, Zhang Q. CIP2A is overexpressed in human endometrioid adenocarcinoma and regulates cell proliferation, invasion and apoptosis. *Pathol Res Pract*. 2018;214(2):233-239.

Yue Z, Shen JJ, Huang QT, Qin YF, Li XN, Liu GB. [MiR-135b promotes proliferation of endometrial carcinoma cells by targeting FOXO1]. *Nan Fang Yi Ke Da Xue Xue Bao*. 2016;36(5):675-80. Chinese.

Zanotti L, Bignotti E, Calza S, Bandiera E, Ruggeri G, Galli C, Tognon G, Ragnoli M, Romani C, Tassi RA, Caimi L, Odicino FE, Sartori E, Pecorelli S, Ravaggi A. Human epididymis protein 4 as a serum marker for diagnosis of endometrial carcinoma and prediction of clinical outcome. *Clin Chem Lab Med*. 2012;50(12):2189-98.

Zhao C, Wang G, Zhu Y, Li X, Yan F, Zhang C, Huang X, Zhang Y. Aberrant regulation of miR-15b in human malignant tumors and its effects on the hallmarks of cancer. *Tumour Biol*. 2016;37(1):177-83.

Zhao T, Su Z, Li Y, Zhang X, You Q. Chitinase-3 like-protein-1 function and its role in diseases. *Signal Transduct Target Ther*. 2020;5(1):201.

La borsa di dottorato è stata cofinanziata con risorse del
Programma Operativo Nazionale Ricerca e Innovazione 2014-2020 (CCI 2014IT16M2OP005),
Fondo Sociale Europeo, Azione I.1 "Dottorati Innovativi con caratterizzazione Industriale"

UNIONE EUROPEA
Fondo Sociale Europeo